Heletz experimental site overview, characterization and data analysis for CO2 injection and geological storage

Citation for published version:
Niemi, A, Bensabat, J, Shtivelman, V, Edlmann, K, Gouze, P, Luquot, L, Hingerl, F, Benson, SM, Pezard, PA, Rasmusson, K, Liang, T, Fagerlund, F, Gendler, M, Goldberg, I, Tatomir, A, Lange, T, Sauter, M & Freifeld, B 2016, 'Heletz experimental site overview, characterization and data analysis for CO2 injection and geological storage', *International Journal of Greenhouse Gas Control*, vol. 48, pp. 3-23. https://doi.org/10.1016/j.ijggc.2015.12.030

Digital Object Identifier (DOI):
10.1016/j.ijggc.2015.12.030

Link:
Link to publication record in Edinburgh Research Explorer

Document Version:
Peer reviewed version

Published In:
International Journal of Greenhouse Gas Control

Heletz experimental site overview, characterization and data analysis for CO_2 injection and geological storage

Auli Niemi[1], Jacob Bensabat[2], Vladimir Shtivelman[3], Katriona Edlmann[4], Philippe Gouze[5], Linda Luquot[5,6], Ferdinand Hingerl[7], Sally M. Benson[7], Philippe A. Pezard[5], Kristina Rasmusson[1], Tian Liang[1], Fritjof Fagerlund[1], Michael Gendler[3], Igor Goldberg[3], Alexandru Tatomir[8], Torsten Lange[8], Martin Sauter[8] and Barry Freifeld[9]

1. Department of Earth Sciences, Uppsala Universitet, Villavägen 16B, Uppsala 75236, Sweden
2. Environmental and Water Resources Engineering – EWRE Ltd., PO Box 6770, Haifa 31067, Israel
3. The Geophysical Institute of Israel, P.O.Box 182, Lod 71100, Israel
4. School of Geoscience, Grant Institute, The King's Buildings, University of Edinburgh, James Hutton Road, Edinburgh, EH9 3FE. United Kingdom.
5. CNRS Geosciences Montpellier, Universite de Montpellier, Campus Triolet CC060, Place Eugene Batalluon, 34095 Montpellier Cedex05, France
6. Consejo Superior de Investigaciones Cientificas, CSIC, IDAEA, Pascual Vila building, office 625 C/ Jordi Girona, 18-26, 08034 Barcelona, España
7. Stanford University, Global Climate and Energy Project, Jerry Yang & Akiko Yamazaki Environment & Energy Building 4230, 473 Via Ortega, Stanford, CA 94305, USA
8. Angewandte Geologie, Universität Göttingen, Goldschmidtstr. 3, 37077 Göttingen, Germany
9. Class VI Solutions, Inc., 711 Jean St. Oakland, CA 94610, USA

*Corresponding author (TEL: +46 18 471 2263, E-mail: auli.niemi@geo.uu.se)

Abstract

This paper provides an overview of the site characterization work at the Heletz site, in preparation to scientifically motivated CO_2 injection experiments. The outcomes are geological and hydrogeological models with associated medium properties and baseline conditions. The work has consisted on first re-analyzing the existing data base from ~ 40 wells from the previous oil exploration studies, based on which a 3-dimensional structural model was constructed along with first estimates of the properties. The CO_2 injection site is located on the saline edges of the Heletz depleted oil field. Two new deep (>1600 m) wells were drilled within the injection site and from these wells a detailed characterization program was carried out, including coring, core analyses, fluid sampling, geophysical logging, seismic survey, in-situ hydraulic testing and measurement of the baseline pressure and temperature. The results are presented and discussed in terms of characteristics of the reservoir and cap-rock, the mineralogy, water composition and other baseline conditions, porosity, permeability, capillary pressure and relative permeability. Special emphasis is given to petrophysical properties of the reservoir and the seal, such as comparing the estimates determined by different methods, looking at their geostatistical distributions as well as changes in them when exposed to CO_2.

Keywords

Deep geologic storage of CO_2, site characterization, site properties, CO_2 injection

1. Introduction

The Heletz site in Israel has been developed for scientifically motivated CO_2 injection experiments with the objective of improving our understanding of the fate of the geologically stored CO_2, including processes of CO_2 spreading and trapping in geological formations. In addition, testing of the rapidly evolving technological and methodological advances related to in-situ monitoring, laboratory testing and modeling are envisioned as a part of the projects at the Heletz site. The first of the planned CO_2 injection experiments are described in Fagerlund et al. (2013a,b) and Rasmusson et al. (2014)) and will address in-situ measurement of residual and dissolution trapping. These are planned to be followed by experiments related to effects of impurities in the gases of the injected CO_2 stream (Jung et al., 2016, this issue) and testing of different modes of injection to enhance the trapping. The objective of all of these experiments is to gain understanding of various process, not to actually store CO_2 in larger scale. Altogether some thousands of tons of CO_2 will be injected into the relatively thin target layer with a thickness of the order of ten meters, at the depth of about 1,6 km. The site is part of Heletz oil reservoir that had been developed and explored for oil exploration purposes. Therefore, a large number of deep wells have previously been drilled over a relatively small area, providing substantial geological information. The CO_2 injection site was selected to be situated in a part of the Heletz reservoir were no oil was found and is located on the saline edges of reservoir. The conditions therefore represent those of a saline aquifer. The experimental site has been primarily developed in the framework of the EU FP7 projectMUSTANG (www.co2mustang.eu) and continued in the ongoing EU FP7 projects TRUST and CO2QUEST.

This paper provides a description of the characterization work carried out for the site, with particular focus on properties related to CO_2 injection. The objective is two-fold. First objective is to provide an overview of the site characteristics, thereby adding to our understanding of properties of potential CO_2 storage aquifers. The second objective is to provide a coherent data-base and conceptual model that can be used by different groups in their further analyses, modeling studies and other studies related to the Heletz site in particular and even for more generic CO_2 injection related studies. While this paper provides an overview of the field work and laboratory analyses carried out in terms of characterizing the site, in particular in the vicinity of the proposed injection area, several of the other papers in this same special edition address the related laboratory findings in detail (Edlmann et al, 2016, this issue, Elhami et al. 2016, this issue, Hingerl et al. 2016, this issue, Luquot et al. 2016, this issue, Soler et al. 2016, this issue, Tatomir et al. 2016, this issue)

Site characterization is an essential step in assessing a site for CO_2 injection and storage, in quantifying its relevant properties and enabling model predictions, risk assessments and interpretations of the monitoring. While site characterization methodologies are commonly known and used in the CO_2 storage projects, they appear to receive relatively little attention in CO_2 geological storage literature, including the Best Practices Manuals, in comparison to e.g. monitoring techniques (for overview, see e.g. Niemi et al, 2014b). In the European perspective, detailed instructions on what should be addressed in a CO_2 storage project are given in the EU directive for the characterization and assessment of a potential storage complex (EU, 2009). In this directive, site characterization is defined in a wide sense and divided in the three steps: (i) data collection, (ii) building a 3-dimensional model and (iii) characterization of the storage dynamic behavior, sensitivity characterization and risk assessment. From the US perspective, NETL (2010, 2013) in the report 'Best Practices for: Site screening, Site selection and Initial Characterization for Storage of CO_2 in Deep Geologic Formations' divides the steps of characterizing a potential CO_2 storage site to four stages: (i) site screening, (ii) site selection, (iii) initial sharacterization, which expands the data analysis of site selection and finally, (iv) site characterization to develop a more detailed characterization of the site. This could include additional drilling and testing of wells, to analyze geochemical and geomechanical properties, including stimulation testing to analyze injectivity, as well as additional seismic surveys. In addition to the existing guidelines/regulations, it can be mentioned that work is presently ongoing to develop ISO standards to cover these area, an additional mechanism of formalizing methodologies.

In this paper we present and discuss the set of studies performed for characterizing the Heletz site with particular focus on the zone where small-scale CO_2 injection experiments are to be carried out. The first stage of the work has consisted of re-analyzing the existing data from oil exploration studies for the new objective of CO_2 injection. Then more detailed data from the injection site has been collected and analyzed, including data from two new wells specifically drilled for the purpose of the CO_2 injection experiments. In the following, we will first describe the site, the data acquisition process and the data sets (Section 2), then we will provide an analysis of the data in terms of the site properties (Section 3) and conclude with an overview, including an outlook to planned activities.

2. Description of the Site and Data Collection

2.1 Description of the Site

The Heletz site, located in the Southern Mediterranean Coastal Plain of Israel, is part of the Heletz oil field discovered in 1955. It has subsequently been developed by means of ~ 90 wells, ~ 40 of which are within the Heletz structure. The structure is an anticline fold with a crest of about 2 km by 4 km and with a vertical closure of 70 m, gently dipping to the east, truncated by a pinch-out line to the west and subdivided into a number of blocks by transversal normal faults with small displacements. The reservoir consists of three Lower Cretaceous sand layers, belonging to the Heletz Formation of the Kurnub group. In the wells located in the central parts of the structure the sands are oil producing, while in several wells located at flanks of the structure they are saturated by salt water (Figure 1). The potential reservoir units for CO_2 injection consist of three sand layers K, W and A (Figure 2), that are separated by shales of varying thicknesses. The lateral extension of the layers is limited to the west by a pinch-out line westward where the sands are replaced by shales. The sand reservoir has its top at the depths of -1370 m to -1560 m and bottom at -1404 m to -1587 m (Figure 1). The total reservoir thickness increases from 2.2 m near the pinch-out at the north-west to 20.6 m at the south-east, at the limits of the explored area. The sand reservoir is overlaid by a limestone layer which is the main geological marker in the area, and above that a thick impermeable shale and marl interval which probably has served as a cap-rock for oil accumulation. The thickness of the cap-rock increases from 23 m in the north to 54 m in the south.

The site selected for CO_2 injection is located at the north-eastern edges of the depleted field, in the vicinity of well H-18 (Fig 1.). The location was selected based on two criteria: firstly, there should be no presence of oil and second, reliable prior information had to be available from previous well analysis and testing, including an abandoned well with potential for re-entry. The original plan was to re-enter an existing well for the purpose of the CO_2 injection experiments. The re-entry attempts failed and finally two new wells were drilled for the experiments (see Section 2.3).

In the experimental area, the reservoir comprises a limestone layer (LC-11) and the three sandstone layers K, W and A of the Heletz sandstones (Fig 2.). The reservoir is bounded from above by a relatively thick layer of shale and marl. The layer thicknesses are of up to 28 meters for LC11, 3 meters for sand layer K, 4 meters for sand layer W and 10 meters for A. Initially all of these layers K, W and A were selected as target layers for the injection as they were extensively investigated for oil exploration and substantial information was available about their properties. Later on, based on the more detailed investigations, layer K was excluded from the injection experiments and was not perforated (Section2.3.2).

2.2 Data available from oil exploration studies and their analysis

Prior to any field activity for the CO_2 injection experiments, existing data from previous oil exploration studies and wells, in particular the ~ 40 wells within the Heletz structure, were analyzed. This was done in order to create an up-to-date picture of the site geology, layer thicknesses and topography, the relevant hydraulic properties (porosity, permeability), chemical composition of the formation water, as well as cumulative thickness of the conductive layers and of the cap-rock.

2.3 Data collected for the CO_2 injection studies

Based on the criteria set for selecting the area for the CO_2 injection studies (Section 2.1), as the first choice the oil exploration well H-18 was selected for a re-entry attempt. The well had been drilled in the 1950's down to the target layers, the "Heletz sandstones", but did not show any oil and was therefore abandoned. The findings from this well allowed its vicinity to be selected for the CO_2 injection experiments, as it could be expected that there would be very little or no oil present and there was good information on the local geology. Following a serious attempt to re-enter the well H-18 (Niemi et al, 2014a), it had to be concluded that the well was not suitable for re-entry. The re-entering failed as it was not possible to drill through the well plug (placed into the well when it was found non-producing) as the drill head repeatedly hit what turned out to be highly corroded casing in a section that had to be passed first, a perforated section into saline karst aquifer (for details see Niemi et al, 2014a)

Therefore, two new deep (~1650 m) wells were drilled near H-18, for the purpose of the CO_2 injection experiments (Figure 1b): i) Heletz 18-A, destined for injection, water abstraction and monitoring, and ii) Heletz 18-B, destined for monitoring and fluid abstraction. The exact positions of the target layers in these boreholes are provided in Table 1. From and around these wells a characterization program for the purpose of future CO_2 injection was carried out during 2012-2014, including:

1. Coring and extensive core analysis of the reservoir and the caprock on core samples from both wells;
2. Fluid sampling;
3. Collecting and analyzing geophysical log data from the wells;
4. 3D seismic survey;
5. In-situ hydraulic testing;
6. Measurement of the baseline pressure and temperature in the reservoir.

In addition, tracer testing and thermal recovery testing will be carried out later, as part of the CO_2 injection experiments, as described in Rasmusson et al. (2014).

2.3.1 Coring and core analysis

Cores were taken from the reservoir and from the cap-rock in both wells. Example of a core log along with the geological interpretation is given in Figure 3a. The full core logs for all sections are summarized in MUSTANG Deliverables (Bensabat et al., 2014, Edlmann et al, 2015). Cores from the cap-rock were embedded in epoxy resin in order to protect them from chemical and mechanical alterations (Figure 3b). Samples of these cores were sent to different laboratories for analysis; in particular (i) for the determination of the capillary pressure and relative permeability curves (Hingerl et al, 2016, this issue); (ii) for a detailed analysis of the caprock and its alteration when exposed to CO_2, and testing of the properties of the reservoir rock (Edlmann et al, 2016, this issue), (iii) for the execution of flow-through experiments and determination of chemical reactivity of the reservoir rocks (Luquot et al, 2016, this issue); (iv) for the determination of the mechanical properties (Eshasi et al, 2016, this issue) and (v) for visualization of the structure and detailed measurement of the hydraulic properties, in particular porosity and permeability (Tatomir et al, 2016, this issue). The overall objective of the core testing has been to determine the petrophysical, mechanical and hydrodynamical properties of the reservoir rock and caprock as well as to evaluate the possible changes of the hydrodynamical properties due to the injection of the CO_2. In addition, the behavior of the caprock in case of leaky fractures has been analyzed (Edlmann et al, 2016, this issue). In general, the core analyses indicated a poor cementation of the reservoir layers.

2.3.2 Geophysical logging and baseline seismic surveys

A comprehensive set of geophysical logs was conducted in both wells, including electrical resistivity, natural gamma radioactivity, density, neutron porosity, spontaneous potential (SP) and two-arm caliper. The logs were interpreted by Israel Geophysical Institute GII and CNRS and provided some key information: 1) the layer structure is consistent with the picture that was built based on previously available data; 2) the “K”, “W” and “A” layers could all be considered suitable for injection based on low shale content, high interpreted porosity and the presence of a 60 mV SP anomaly (Figure 4) indicative of high permeability of the sand layers to mud filtrate during drilling. The vertical fractures detected from dual laterolog resistivity analysis (Pezard and Anderson, 1990) above the reservoir are in accordance with BHTV and breakout analyses in boreholes from the nearby Kokhav field (Amiel, 1991), who concludes the presence of a strike-slip to normal faulting in-situ stress regime for the Kokhav field, less than 10 km from Heletz. No particular fracturing was, however, detected in the sand reservoirs of the new holes drilled (Figure 4). Based on the results of these log analyses and in particular considering layer thicknesses, only the W and A layers were perforated when the wells were instrumented for injection and monitoring (Section 2.4). Examples of logs (analyzed with Techlog (Schlumberger™) program) are given in Figure 4, while the full logs are to be found in Bensabat et al., (2014).

A 3D seismic survey in order to prepare a baseline picture of the reservoir and to identify the reservoir and cap-rock units was carried out by the Geophysical Institute of Israel (GII) The results confirmed the earlier models of the site and are documented in Bensabat et al. (2014) and Niemi et al. (2014).

2.3.3 Hydraulic and geochemical characterization

To determine the in-situ hydraulic conductivity of the reservoir layers, an in-situ pumping test was conducted in the injection well. The test was carried out as a single-well test with pumping and pressure monitoring in the same well. The test was implemented by introducing a submersible pump in the well (at a depth of ~270 m) and conducting a pump and recovery test, automatically measuring the drawdowns and the pump discharge. The result of this test gives an integrated value over layers A and W. During the pumping test in the injection wells water samples of the produced water were collected and sent for comprehensive chemical analyses.

2.4 Monitoring system

The new wells H-18A and H-18B were instrumented for water and CO_2 injection, fluid withdrawal, fluid sampling and various measurements, for the purpose of the actual injection experiments. This equipment has been used for establishing some of the baseline conditions as well. The instrumentation of the injection well H-18A (Figure 5a), includes: 1) pressure and temperature sensors at the top and bottom of the perforated area; 2) a tube-intube fluid sampling system, a further development of the U-tube (Freifeld et al, 2005); and 3) a hybrid copper/optical fiber cable for performing distributed heat pulse and acoustic sensing. H-18A includes also a chemical injection line, connected to the injection tubing at a depth of 1000 meters. It allows the mixing of the fluid injected in the tubing (either water or CO_2) with tracers, impurities and or CO_2 (for saturation purposes). The instrumentation of the monitoring wells, H18B (see Figure 5b), is similar to the one in the injection well, with the exception of the chemical injection line. Water withdrawal from both wells is via airlift. Figure 5c also show the well-head of the injection well, along with the various sensor and sample lines that are connected to the control room. The control room contains the U-tube sampling collection panel, which allows collection of downhole fluid samples, either under the formation pressure conditions or depressurized. The panel has been supplemented with an equipment for the measurement of the partial pressure of the gases, electrical conductivity of the sample and its pH. This allows the determination, almost in real time, the mass of CO_2 dissolved in the brine and as free phase. The control room is equipped with a mass spectrometer allowing onsite determination of the concentration of gases that are used as tracers. Additional facilities include computers for the collection and storage of the pressure and temperature data, temperature information from the optical fiber, and seismic data from three shallow seismic monitoring wells.

3. Data analysis

3.1 Three-Dimensional Geological Model of the Site

The 3D structural model produced for the site describes the main geological features of the reservoir and cap rock layers based on data from about 40 wells located within the Heletz structure. The full geological model including all the maps and cross-sections is not reproduced here for space considerations but can be downloaded as an EU project deliverable report (Erlström et al, 2010 and 2011) from the MUSTANG project web-site www.co2mustang.eu. In the following we will only give example maps and cross-sections to describe the main features of the site. The spatial extent of the model is limited to the Heletz oil field (~5.5 km by 4.0 km) within the depth interval of -1300 to -1600 m. The model and maps were produced by the GII team using HDS software for well log analysis and Golden software Surfer, Strater and Grapher for geological mapping.

Structure maps were built for the top of the cap rock and top and bottom of the sand reservoir. The structure maps show the geometrical features of the corresponding surfaces, well locations, pinch-out lines, faults and oil-water contacts. As an example, Figure 1 shows the elevation of the base of the sand reservoirs. Isopach maps were built for seven units: the cap rock, the limestone LC-11 layer, the three sand layers K, W and A as well as the total sand reservoir. As an example, the isopach of the thickest and major sand layer A is given in Figure 6. The sand reservoir has its top at the depths of -1370 m to -1560 m and base at -1404 to -1587 m. The reservoir is overlaid by a limestone layer LC-11 with a thickness of 1–10 m, with a local anomaly of 28 m in the vicinity of the H-24 well near the pinch-out line. The thickness of the uppermost sand layer K varies between 0.6 m in south-western part of the structure to 2.8 m on the crest of the structure. This layer was not present in the southern part of the structure. The lateral extent of the middle sand layer W is very limited as compared to the two other sand layers and is located mainly in the eastern flank of the structure where its thickness increases from 1 m at the west to 5.8 m in the east. The bottom sand layer A shows a clear south-eastern trend and its thickness varies between 2.2 m and 14.6 m. The cap rock lies in the depths of -1295 m to -1518 m and its thickness increases from 23 m at the north to 54 m at the south, with a local anomaly of 62 m in the northern part of the structure in the vicinity of the H-25A well. All the above depth levels are given in meters below mean sea level, as customary in these types of maps. The level of land surface at the site is about 114 m above the m.s.l. For the borehole measurements to be discussed below, the reference point is the drilling rig (the so called kalibush) which is 117,73 meters above the mean sea level. As the land surface is 114 m above m.s.l. the borehole depths to be discussed later are close (within a precision of about 3 meters) to the actual depth from the land surface, while to the values discussed above given in m.s.l one needs to add about 114 m to get the depth from land surface (in the vicinity of H-18)

Several geological cross-sections were also constructed (Erlström et al, 2010) giving an overview of the extent, thickness and continuity of the various layers. The cross-sections show the location and the total depth of the wells, geometry, lithology and stratigraphy of the reservoir, overlying and underlying layers; and also oil-water contacts and faults. Within the sand reservoir, the type of fluid content in each layer is indicated by different colors. As an example, cross-section A-A crossing the CO_2 injection area and the well H-18, chosen as the first candidate for the re-entry for the CO_2 injection experiment is shown in Figure 7.

While all the information concerning the 3D geological model of the entire Heletz site is available in above deliverables (Erlström et al, 2010 and 2011), the remainder of this paper will focus on the experimental area near the CO_2 injection site (Figure 1).

3.2 Baseline Pressure and Temperature

Information about the in-situ pressure and temperature was available earlier e.g. from wells H-25 and H-37 (Table 2) indicating pressure values in the range of 132-136 bars and temperatures between 61 to 65 ℃. With the installed monitoring system for the CO_2 injection experiments, the pressure and temperature in the vicinity of wells H-18A and H-18B was measured. Pressure and temperature values from these wells are ~143 bar and 64 ℃.

3.3 Mineralogy

The mineralogy of the samples has been determined using X-ray diffraction (XRD). Figure 8 presents the average XRD mineralogy results for the cap-rock and sandstone samples. The corresponding numerical values are presented in Table 3 and some of the corresponding petrophysical data in Table 4. The main minerals for the cap-rock are K-feldspar, plagioclase, kaolinite, muscovite, illite, when determined for samples from the new wells H-18A and B. For samples form one of the old wells, H-2 they are kaolinite, muscovite, illite, microcline, orthoclase, chlorite and quartz. It can be seen that the main minerals for the reservoir rock are quartz and K-feldspar while the minor minerals are kaolinite, illite, plagioclase, pyrite, dolomite chlorite, siderite muscovite and ankerite. The expected changes of the mineral composition when in contact with CO_2 and/or CO_2 rich brine are discussed in overview in Section 3.9 of this work and described in detail in Luquot et al, (2016, this issue) and Edlmann et al. (2016, this issue).

The sandstone proved to be very poorly consolidated and both sandstone cores disintegrated during vacuum saturation with 35,000ppm NaCl equivalent brine, in a specific test carried out by the University of Edinburgh. This disintegrating behavior was observed by other laboratory groups as well, and special techniques were needed in the subsequent testing.

3.4 Water Chemistry

Water quality data was available previously from 1955 from oil exploration studies from the nearby old well H-18. During the hydraulic testing (Section 2.3.4), new water samples were taken from the well H-18A and sent for chemical analysis. The results (shown in Table 5) are very similar to the old water quality data from 1957 from the nearby well H18 (see Bensabat et al, 2011), thereby providing confidence in their representativeness The concentration of suspended solids is very high (~60g/l). Presence of hydrocarbons was detected in the geophysical log interpretation (Figure 4 and section 2.3.2) in discrete and meter thick layers of the K, W and A reservoirs, with volumes of 2 to 6 %.of the pore space (porosity).

Strontium isotope analysis of the sandstones performed by LIAG (Leipzig Institute for Applied Geophysics) and University of Göttingen as part of their work on rock cores (see Tatomir et al, 2016, this issue) indicated that the fluid–rock interactions in the reservoir are in equilibrium. This in turn indicates that there is no communication with other compartments or some groundwater flow.

3.5 Porosity

3.5.1 Reservoir porosity

First estimates of the porosity and permeability for the reservoir layers were made based on the data from 41 oil exploration and water wells, mainly from geophysical (electrical, density, acoustic and neutron) logs and also from available core information. The approach used was as follows; (i) the target reservoir layers and the cap-rock were identified and the corresponding layer boundaries on all relevant well logs were established; (ii) the results were checked by correlation with adjacent wells, (iii) porosity of the layers was determined from various logs. This was done by applying Archie's law to electrical logs in water wells, correcting the results for oil wells, (based on estimated oil/water saturation), computing porosity from available acoustic logs and correlating with core analysis. Porosity map obtained this way for the interval W is shown in Figure 9 (similar maps for the other layers to be found in Erlström et al, 2010). The map shows porosities of the order of 15 to 20% in the investigation area and particularly near wells H-18, and overall mean porosities of 18, 20 and 17% for the entire intervals A, W and K, respectively.

From the drilled new wells H-18A and H-18B, porosities were determined based on both geophysical logs (Section 2.3.2) and from several core samples, as part of the core testing program (Section 2.3.1). Example of a geophysical well-log interpretation is shown in Figure 4. Based on these, the porosities for the sand layers were interpreted close to 18±4 %.

Several of the research groups determined porosities from the core samples as part of other investigations. All these core analyses were for samples from the main layer, the A layer. Tatomir et al (2016, this issue) compared different experimental laboratory and imaging CT-based methods to determine porosity and found the porosity to vary between 19-22%. The Stanford group, as part of the relative permeability analyses (Hingerl et al, 2016, this issue) determined porosity values based on MICP analyses in the range of 22-25%. Luquot et al. (2016, this issue) analyzed changes in rock porosity and permeability due to exposure to brine saturated with CO_2 and the initial porosity values of their samples ranged from 15-26%. Edlmann et al (2016, this issue) tested one reservoir sample as part of their cap-rock studies and got a helium porosity value of 28%. Based on these values we can conclude that the porosities in the vicinity of the test wells are in reasonably good agreement with the original estimates from oil exploration studies, but somewhat higher than the overall values for the Heletz layers. It should be pointed out that the estimates in Figure 9 in the vicinity of the wells H-18A and H-18B are based on relatively few wells, so that the recent values can be considered more reliable. Leaving out the most extreme values, it can be concluded that the porosity values from the cores mainly fall in the range of 20-25% in the experimental region, while the geophysical logs show somewhat lower values being of the order of 18±4 %.

The apparent discrepancy between the porosity values measured in the laboratory on the cores and those deduced from well logging may have several origins. First, it may be due to decompression of the fairly loose core material brought to surface from the fairly anisotropic in-situ stress field (Amiel, 1991). This would not be unexpected and highlights the difference between in-situ estimates from logging and surface measurements. Second, there may be bias in the selection of the core samples, because of the difficulty of extracting cores with poor cohesion and the cores may therefore be more representative of clay-free reservoir end-member. Finally there is a possibility for alteration of the cores chemically, by the coring fluid. On the other hand, the measurements in the laboratory are direct measurements, while the geophysical well-logs provide indirect estimates. For ease of comparison all porosity values are summarized in Table 6.

3.5.2 Caprock porosity

No estimates on cap-rock porosity were available from the oil exploration studies. This is not unusual, as the properties of the reservoir layer are typically of more interest. One of the conclusions of the MUSTANG site characterization program where data from five prospective CO_2 injection sites were analyzed was that detailed data concerning cap-rock properties was typically lacking (Erlström et al, 2011). The fact that the cap-rock has held hydrocarbons stored underground does, however, indicate a low permeability. From the new wells H-18A and H-18B cap-rock cores were retrieved and measurements of cap-rock porosity, permeability and some other key properties were performed by the University of Edinburgh group, as part of their work on characterizing the estimated changes of the cap-rock when exposed to CO_2 and brine containing CO_2 (Section 3.9). Their porosity and bulk density values are summarized in Table 4. The porosity values range between 5.75 and 10.8 % and the bulk density between 2.07 and 2.46 g/cc. These are representative of standard shale values (Neuzil, 1994), especially when the mineralogy is taken into account where the presence of kaolinite will account for the slightly lower than expected bulk densities.

3.6 Permeability

3.6.1 Reservoir Rock

From the previous oil investigations no direct permeability measurements were available for the Heletz field. Therefore, in order to get a preliminary understanding of the permeability in the area, a statistical relationship was established in order to evaluate permeability from porosity values estimated from well log data. For this purpose, all available core data were analyzed and, as a result, a set of 120 core samples for which both the porosity and permeability measurements were available was selected to establish a statistical permeability – porosity relationship for the entire Heletz site (Fig 10). This relationship was used to calculate permeability for all wells and interpolated estimates for layers A and W, are shown in Figures 11a and b. The obtained values can be regarded as a first approximation of the true permeability values for the layers. The average layer permeabilities obtained for layers A, W and K were 150 mD, 250 mD and 110 mD, respectively. In the vicinity of the investigation area the values are below 100mD but given the uncertainties in both the porosity-permeability relationship and the interpolation, the expected permeability of the layers prior to the detailed investigations was assumed to be about 100mD, based on the overall values.

From the drilled wells H-18A and H-18B, permeability values were determined based on both testing in the laboratory on core samples and on the in-situ hydraulic pumping test.

The group by LIAG and University of Göttingen carried out a first set of experiments under atmospheric conditions for two distinctly different samples as shown in Table 7 including testing the anisotropy. The results show mean values of 440-450 mD for the fine grained (H-18A) sample and 340-350 mD for the coarse grained sample (H-18B), with essentially no anisotropy at the core level. Later, the same group carried out laboratory permeability tests at in-situ pressure and temperature conditions, including a comprehensive comparison of different permeability measurement methods with somewhat different sub-samples than those in Table 7 (Tatomir et al, 2016, this issue) concluding overall permeability values of the order of 325-410 mD at injection well (H-18A) and 180-295 mD at H-18B. As part of their work to study the effect of CO_2 saturated brine on rock properties Luquot et al. (2016, this issue) determined permeability values prior to the experiments ranging from 100 to 400 mD (five tests in H-18A). In connection to the relative permeability measurements Hingerl et al. (2016, this issue) determined permeability of about 100mD (see also Section 3.8).

The in-situ pumping test carried out in well H-18A provides a field-scale value of permeability for the layers A and W. The drawdown along with the pumping discharge are shown in Figure 12. The interpretation of the test was carried out using the EWRE-SPT software, based on the semi-analytical solution of Moench (1997). The inference of the test resulted in an equivalent horizontal permeability of 735 mD and a vertical permeability of 135 mD. These values are considerably higher than the original estimate, and even higher than the point samples from the recent core analyses. One possible explanation for the difference is the nature of the horizontal anisotropy in the correlation structure. This issue will be discussed in more details in the later chapter where geostatistical properties of the sands porosity and permeability are discussed. Another possible explanation is that the in-situ permeability was somehow increased in the well stimulation effort that was necessary as the well after drilling and prior to hydraulic testing had become clogged. This should in principle not happen and the permeability should not increase beyond the original level but may be possible because of the very fragile nature of the sandstone cement. All the permeability measurements and estimates are summarized in Table 8.

3.6.2 Cap-rock

Concerning the permeability values of the cap-rock, there is a similar lack of data as for porosity. The few measured core values are shown in Table 4. The caprock permeability of 4.4mD is slightly higher than expected (Neuzil, 1994), however this can be explained by the silty nature of the caprock, Figure 3a. The caprock properties and their change when in contact with CO_2/brine are discussed in detail in Edlmann et al (2016, this issue)

3.7 Relative permeability and capillary pressure

Stanford University group (Benson et al, 2015, Hingerl et al, 2016) performed a full characterization of several sandstone layer A cores in terms of mineralogical, textural, physical and especially the multi-phase flow properties. The methods included helium pycnometry, permeability measurement mercury intrusion porosimetry and relative permeability measurements with CT scanner, as described in detail in Benson et al. (2015) and Hingerl et al. (2016). Figure 13 shows the determined capillary pressure – saturation curve. These values are converted from the system mercury-air to the system supercritical CO_2-H_2O. The relative permeability curves for the gas and liquid, including both the drying and imbibition cycles are shown in Figure 14. The fitted model is also shown and the corresponding Brooks and Corey model parameters summarized in Table 9. Corresponding grain densities for the analyzed 6 sub-samples had an average of 2.645 g/cc and an average porosity of 23.5 %. A permeability of 104 mD was measured based on the pressure drop across the core. The measurements and interpretation of the multiphase properties in terms of the mineralogical and other properties of the rock are discussed at depth in Hingerl et al (2016, this issue). In general, the data shows a good gas permeability. The residual CO_2 saturation (the amount of CO_2 trapped as a residual phase) is about 0.2, but varies with the maximum CO_2 saturation obtained before imbibition.

Using somewhat different methods and samples, University of Göttingen group also determined the capillary pressure - saturation relationships by means of mercury intrusion porosimetry performed in the laboratory and with a μCT-based pore-scale model. These experimental and numerical results are discussed in detail in Tatomir et al (2016, this issue).

3.8 Geostatistical properties of the sand layers

The data from the well-logs were also used to get an understanding of the geostatistical distribution of permeability in the sand layers (Figures 15a and b). These permeability distributions are based on the porosity logs collected over the entire area containing 314 (layer W) and 1326 (layer A) data values. These data were converted to permeability distributions using the empirical porosity-permeability relationship in Figure 10b. For layer A, the 41 permeability measurements on core samples that were available were also included into the data set. The corresponding model parameter statistics for both layers are given in Table 10. In the histogram for layer A, the values determined by the new core analyses are also shown, indicating that these fall in a considerably narrower range than the estimate from the porosity-permeability relationship for the entire formation. This may indicate inaccuracies in the adopted porosity-permeability relationship or that there is indeed less variability in the region near wells H-18A and H-18B than in the entire domain, or possibly both. Olofsson (2011) carried out a similar geostatistical analysis based on porosity-permeability data from three old boreholes, H-13, H-18 and H-38, to represent the area near the new wells and the experimental area. The statistics related to this data set are also summarized in Table 10.

Olofsson (2011) also constructed vertical semi-variograms of the data and fitted an exponential variogram model to that. The correlation length was determined to be 2.7 m and the corresponding model parameters are shown in Table 10 as well. The variogram could be considered to be representative, based on the number of data pairs included and the fact that the data variance is well captured by the sill of the variogram. . It should be emphasized that this variogram only applies to the vertical autocorrelation structure. The horizontal correlation length cannot be determined from the available data. A typical assumption in sedimentary formations is that the horizontal correlation length is higher than the vertical one. Our preliminary model analyses calculating effective permeability of heterogeneous formations indicates that with similar model dimensions, mean permeabilities, correlation lengths and standard deviations as those measured for Heletz layer A (Table 10), high standard deviation and high horizontal correlation length, can produce significant anisotropy in the effective permeability of the layer, and similar order of magnitude to that observed in our in-situ well test. To this end, Figure 16 shows results of Monte Carlo simulations of effective permeabilities in both vertical and horizontal directions. Domain size was a 10 m x 100 m vertical cross-section, vertical correlation length was 3 m, horizontal correlation length was varied from 2 m to 30 m and standard deviation (σ) varied from 0.2 to 1. In these simulations the mean of the input permeability values was 100 mD, which was the original assumption for Heletz layers A and W mean permeability. The results in Figure 16 show that high anisotropy (high ratio between the horizontal and vertical permeability) is reached when standard deviation and horizontal correlation length are large. For example, with fixed $\sigma = 0.7$ the highest correlation length (30 m) provides about two times higher horizontal permeability than the vertical one and with fixed horizontal correlation length 30 m and $\sigma = 1.0$, the horizontal value is about three times higher than the vertical one. This result, together with the permeability values measured at Heletz, both from the cores and in-situ, indicates that the horizontal correlation length at Heletz may be significantly larger than the vertical one.

3.9 Changes in mineral composition and petrophysical properties when in contact with CO_2

Extensive laboratory testing was carried out to investigate the changes in rock composition and petrophysical properties when in contact with brine containing dissolved CO_2. The experiments were carried out at in-situ pressure and temperature conditions and are described in detail in Luquot et al. (2016, this issue) and Edlmann et al. (2016, this issue), for the reservoir rock and caprock, respectively.

For the reservoir rock, CNRS carried out experiments where CO_2 rich brine was injected through re-compacted core samples at in-situ conditions of T=60 ℃ and P=15 MPa. Different flow rates and brine compositions of the injected solution were tested. The experiments were carried out with Heletz brine equilibrated with gypsum to evaluate the consequences of gypsum precipitation. Gypsum precipitation is locally expected due to the presence of Ca in some of the minerals present and to the fact that the brine composition is already near the gypsum equilibrium (Tables 3 and 5). As described in detail in Luquot et al (2016, this issue) the permeability increased for most of the experiments (Figure 17), and the increase is faster with the higher flow rate. Based on the related mineralogical studies (Luquot et al., 2016), the increase in permeability was related to localized dissolution and precipitation processes, in particular dissolution of dolomite and ankerite and local precipitation of gypsum and clays (kaolinite and smectite). These authors have concluded that carbonate dissolution occurs at (and promotes the development of) fast flow paths, whereas most precipitation concentrates at low flow regions (excepted for gypsum where precipitation reaction is fast). They also observed that precipitation of the secondary minerals with low reaction rates (kaolinite, muscovite and smectite) as well as K-feldspar dissolution is larger at low flow rates than at high flow rates. This behavior can be explained by diffusive mass transfer and dissolution/precipitation localization into immobile zones where local chemical micro-environments develop. These mechanisms are also studied in detail emphasizing the role of the local hydrodynamic properties and mineralogical heterogeneities in Soler et al. (2016, this issue).

For the cap-rock, the University of Edinburgh carried out experiments where Heletz caprock samples were exposed to CO_2 rich brine at 55^oC (please note that this temperature is somewhat too low in comparison to the real in-situ temperatures in the wells, which at the time of initiating the laboratory work was not yet known to the group and the value was approximated from general literature). As described in detail in Edlmann et al (2016, this issue) the mineralogical investigation reveals that the Heletz caprock samples have a relatively simple chemical composition. The primary mineral is K-feldspar (ranging between 30-50 wt%) followed by plagioclase feldspar (6-18 wt%) and kaolinite (7-23 wt%), then illite (2-11wt%) and muscovite (2-11%). Looking at the expected thermodynamic reactivity of the minerals within the CO_2 / formation brine / Heletz caprock series, the high percentage of feldspar would suggest possible reactivity of the Heletz caprock samples on contact with CO_2 saturated brine, but experimental observations on the

Heletz samples indicate that this is not the case. After 3 months exposure to CO_2 saturated brine under in-situ reservoir temperature the Heletz H-2 caprocks remain relatively unchanged, with no significant changes in the weight % of plagioclase feldspar, kaolinite, siderite, dolomite, ankerite and K-feldspar minerals and that no new minerals were observed to have been precipitated during CO_2, brine or heat exposure in the Heletz cap rock samples, Figure 18. There was an observed elevation in the weight % of illite, however there was no corresponding Plagioclase feldspar or K-feldspar decrease, suggesting the reactive mass balance is not at play and the increase in illite is an artefact of sampling in a heterogeneous mudstone. This confirms analogue studies (Baines and Worden, 2004, Haszeldine et al., 2005, Pearce 2006, Lewicki et al. 2007 and Hellevang et al., 2011) that suggest that if the reactive aluminosilicate minerals (such as feldspars, clay minerals, micas, chlorites or zeolites) has been exhausted through natural weathering / diagenesis then no further reactivity will occur.

4. Discussion and Conclusions

This work has provided an overview of the characterization work carried out at the Heletz site, a site developed for scientifically motivated small-scale CO_2 injection experiments. The work has consisted of first re-analyzing the existing data from the previous oil exploration studies and then focusing on the more detailed data from the injection site, including data from the two new wells drilled for the injection experiments. Overall, the investigations from the new wells, including geophysical loggings and geological logs, showed results consistent with the previous understanding on site properties and the locations of the target layers.

At the two investigation wells, the reservoir layers to be used for the injection have a total thickness of 11-13 m, divided into two separate layers. The depth of reservoir top and base at the wells are at 1621 m – 1627 m and at 1635 m - 1641 m, respectively. The reservoir layers have good permeability. Laboratory tests provided values in the range of 100 mD - 410 mD, with somewhat higher values in the injection well in comparison to the monitoring well. The in-situ well test in the injection well provided horizontal/vertical permeabilities of 735 mD/135 mD. A possible explanation to the higher in-situ value can be anisotropy in the correlation structure, as discussed above. Relative permeability and capillary pressure curves were determined as well, indicating good gas relative permeability. Porosity, in turn, is estimated to be of the order of 18±4 % from borehole logs, and of the order of 20-25% from the laboratory tests. Overall, a porosity value of the order of 20% can be taken as representative overall value. To enable the study of heterogeneity effects, geostatistical properties of the permeability were also determined, based on well-log porosity data converted to permeability. The standard deviation of (log transformed) permeability decreases when the size of the domain under consideration decreases, being of the order of 1.1 for the entire Heletz formation and 0.7 for the area in the vicinity of the experimental area. A vertical correlation length of 2.7 was determined based on variogram analysis.

For the sandstones, Strontium isotope analyses showed the fluid–rock interactions in the reservoir to be in equilibrium, indicating that there is no communication with other compartments or groundwater flow. The sandstone proved to be very poorly consolidated and the sandstone cores disintegrated during vacuum saturation with 35,000ppm NaCl equivalent brine. This disintegrating behavior was observed by other laboratory groups as well, and special techniques were needed in various testing for this reason.

Concerning the expected changes of the reservoir rocks when in contact with CO_2, the permeability increased for most of the experiments carried out. The increase was related to localized dissolution and precipitation processes, in particular dissolution of dolomite and ankerite and local precipitation of gypsum and clayes. Carbonate dissolution occurs at and promotes the development of fast flow paths, whereas most precipitation concentrates at low flow regions.

The reservoir rock is from above limited by a cap-rock with a thickness between 23 m (in the north) and 54 m (in the south). The fact that it has contained hydrocarbons for long periods of time speaks for low permeability in general, but no porosity or permeability values were available from the oil exploration studies. From the new wells porosity values of 6-11% were determined and are representative of standard shale values of similar mineralogy. Only one permeability value was determined for the cap-rock and evaluation of the representativeness of this single value requires additional measurements, with other cores and possibly in-situ. Presently, further testing of the cap-rock samples is in progress at two laboratories, in connection to rock mechanical studies. The expected changes of the caprock when in contact with CO_2 were tested in the laboratory, at in-situ pressures and temperatures, and the conclusion from these investigations was that the Heletz caprock contains very few minerals that are likely to react with CO_2 and those that are available have already been subjected to diagenesis and the supply of reactive minerals exhausted. As such the caprock could be considered non-reactive to the underlying CO_2 plume.

In terms of the outlook to the future, it can be concluded that the Heletz site has now been extensively characterized for CO_2 injection and storage properties, by going through both the standard as well as some more advanced, research level evaluation processes. The site characteristics are sufficiently understood to make reliable predictions concerning the coming injection experiments. Several modeling studies for the purpose of planning the injection experiments have already been carried out (Rasmusson et al, 2014, Fagerlund et al., 2013, Jong et al., 2016) and more are underway. The site is ready and instrumented with state of the art monitoring technologies. Installed facilities above the ground allow the injection of CO_2 at different temperatures, injection of water, fluid abstraction and injection of tracers in the water and or the CO_2. The site is operational and work is in progress to carry out the CO_2 injection experiments, with the objective to study different modes of CO2 trapping in-situ, for checking monitoring technologies, assessing the reliability of predictive models and validating them

Acknowledgments

The main funding to this work has come from EU FP7 projects MUSTANG and TRUST, grant agreement numbers 227286 and 309067, respectively. Authors from Uppsala University also acknowledge support from the Swedish National Research Council's (VR) strategic energy research fund. Stanford funding was provided by the Global Climate and Energy Project. Schlumberger is thanked for providing the TechLog platform to Montpellier University for research and training.

References

Amiel Y. 1991. In-situ tectonic stresses and subsurface fractures in Israel. M.Sc. Thesis, Hebrew University, Jerusalem.

Baines, S. J. & Worden, R. H. (eds) 2004. Geological Storage of Carbon Dioxide. Geological Society, London, Special Publications, 233, 59-85. The Geological Society of London 2004.

Bensabat, J., A. Niemi, C. Juhlin. F. Fagerlund, N. Enescu, K. Rasmusson, M. Sauter, I. Ghergut. T. Licha, J. Carrera, G. Wiegand, V. Shtivelman, I. Goldberg, M. Gendler, L. Fleisher. (2011) Report on the experiment planning and preparations. MUSTANG (A multiple space and time scale approach for the quantification of deep saline formations for CO_2 storage) EU FP7 project report, Deliverable D6.1. Sept. 2014. Available at: http://www.co2mustang.eu

Bensabat, J., A. Niemi, P.Gouze, L.Luquot, P.Pezard, K.Edlmann, C. McDermott, V.Shtivelmann, F.Fagerlund, K.Rasmusson, M.Rasmusson, T.Lange, A. Tatomir, M. Sauter, R.Mahmut, S. Benson, F. Hingerl, R. Pini, B. Freifeld, S. Wall, H. Bland et al. 2014. Report on the Injection Experiment. MUSTANG (A multiple space and time scale approach for the quantification of deep saline formations for CO_2 storage) EU FP7 project report, Deliverable D6.3. Sept. 2014. Available at: http://www.co2mustang.eu

Benson, S., Hingerl., F., Zuo, L., Pini, R., Krevor, S., Reynolds, C., Niu, B., Calvo, R., Niemi, A. 2015. Relative permeability for multi-phase flow in CO_2 reservoirs -

Part II: resolving fundamental issues and filling data gaps. A research report prepared for the Global CCS Institute by Stanford University, June 2015. Available at http://www.globalccsinstitute.com/

Edlmann, K. 2015. Heletz H-18 core logging report. MUSTANG (A multiple space and time scale approach for the quantification of deep saline formations for CO_2 storage) EU FP7 project report, Deliverable D4.8. July 2015. Available at: www.co2mustang.eu

Edlmann, K., A. Niemi; J.Bensabat; S.Haszeldine; C.McDermott. 2016, this issue. Mineralogical investigation of the caprock of the field scale experimental CO_2 injection site, Heletz, and its reactivity to scCO_2 injection. Paper under review for the MUSTANG/Heletz Special Edition of International Journal of Greenhouse Gas Control. In review.

Elhami, E., M. Ask and H. Mattsson.. 2016, this issue. Physical- and geomechanical properties of a drill core sample from 1.6 km depth at the Heletz site in Israel: some implications for reservoir rock and CO_2 storage. Paper under review for the MUSTANG/Heletz Special Edition of International Journal of Greenhouse Gas Control. In review.

Erlström, M., O. Silva, L.M., Vries, V. Shtivelman, M. Gendler, I. Goldberg, D. Scadeanu, C. M. Sperber. 2010. 3D structures of the Test Sites. Deliverable D2.2. MUSTANG (A multiple space and time scale approach for the quantification of deep saline formations for CO_2 storage) EU FP7 project report. Nov. 2010. Available at: www.co2mustang.eu

Erlström, M., T. Rötting, C.M. Sperber, V. Shtivelman, and D. Scadeanu and C. M. Sperber. 2011. Report on property values and parameters, related uncertainties. Deliverable D2.3. MUSTANG (A multiple space and time scale approach for the quantification of deep saline formations for CO_2 storage) EU FP7 project report. Deliverable D2.2 July 2011. Available at: www.co2mustang.eu

EU. 2009. Directive 2009/31/EC of the European Parliament and the Council of 23 April 2009, on the geological storage of carbon dioxide and amending Council Directive 85/337/EC, European Parliament and Council Directives 2000/60/EC, 2001/80/EC, 2004/35/EC, 2006/12/EC, 2008/1/EC and Regulation (EC) No 1013/2006 Appendix 1. Criterial for the Characterization and assessment of the potential storage complex and surrounding area referred to in article 4(3)

Fagerlund, F., A. Niemi, J. Bensabat and V. Shtivelman, 2013a. Design of a two-well field test to determine in-situ residual and dissolution trapping of CO_2 applied to the Heletz CO2 injection site. *Int. J. of Greenhouse Gas Control*. 19, 642–651, http://dx.doi.org/10.1016/j.ijggc.2013.01.036.

Fagerlund, F., Niemi, A., Bensabat, J., Shtivelman, V. 2013b. Interwell Field Test to Determine in-situ CO_2 Trapping in a Deep Saline Aquifer: Modelling Study of the Effects of Test Design and Geological Parameters. *Energy Procedia*, 40, 554-563.

Freifeld, B.M., Trautz, R.C., Yousif K.K., Phelps, T.J., Myer, L.R., Hovorka, S.D., and Collins, D. 2005, The U-Tube: A novel system for acquiring borehole fluid samples from a deep geologic CO_2 sequestration experiment, J. Geophys. Res., 110, B10203, doi:10.1029/2005JB003735, 2005.

Haszeldine, R.S., Quinn, O., England, G., Wilkinson, M., Shipton, Z., K., Evans, J., P., Heath, J., Crossey, L., Ballentine, C., J., and Graham, C., M., 2005. Natural geochemical analogues for carbon dioxide storage and sequestration in deep geological porous reservoirs. Oil & Gas Science and Technology - Rev. IFP 60, 33-49.

Hellevang, H., Declercq, J., and Aagaard, P., 2011. Why is Dawsonite Absent in CO_2 Charged Reservoirs? Oil Gas Sci. Technol. – Rev. IFP Energies Nouvelles 66, 119-135.

Hingerl, F., F. Yang, R. Pini, X. Xiao, M. F. Toney, Y. Liu and S. M. Benson. 2016, this issue. Characterization of Heterogeneity in the Heletz Sandstone from Core to Pore Scale and Quantification of its Impact on Multi-Phase flow", Paper under review for the MUSTANG/Heletz Special Edition of International Journal of Greenhouse Gas Control. In review.

Jung, B., J.L. Wolf, D. Rebshcer, R. Segev, J. Bensabat, A. Niemi. 2016, this issue. Hydromechanical and Geochemical Impacts of Impurity on Geological CO_2 Storage at the Heletz Site, Israel. Paper under review for the MUSTANG/Heletz Special Edition of International Journal of Greenhouse Gas Control. In review.

Lewicki, J.L., J.T. Birkholzer, and C.-F. Tsang. 2007. Natural and industrial analogues for leakage of CO_2 from storage reservoirs: Identification of features, events, and processes and lessons learned, Environmental Geology, 52, 457-467.

Luquot, L., Gouze, P., Niemi, A., Bensabat, J. and Carrera, J.2016, this issue. – Laboratory CO_2-rich brine percolation experiments through Heletz samples (Israel): Role of the flow rate and brine composition. *International Journal of Greenhouse gas control*, DOI: 10.1016/j.ijggc.2015.10.023 (2016)

Moench, A.F. 1997Flow to a well of finite diameter in a homogeneous, anisotropic water table aquifer: Water Resources Research, v. 33, no. 6, p. 1397–1407.

Neuzil C.E. 1994. "How permeable are clays and shales". Water Resources Research, Vol. 30, No. 2, Pages 145-150, February 1994

NETL. 2010. NETL SS: Best practices for: Site screening, site selection, and initial characterization for storage of CO2 indeep geologic formations (http://www.netl.doe.gov /technologies/carbon_seq /refshelf/BPM-SiteScreening.pdf

NETL. 2013. NETL SS: Best practices for: Site screening, site selection, and initial characterization for storage of CO_2 in deep geologic formations, 2013 Revised edition.

Niemi, A., et al. (seventy-one co-authors). 2014a. Final Report - Summary of Project R&T Findings. MUSTANG (A multiple space and time scale approach for the quantification of deep saline formations for CO_2 storage) EU FP7 project report. Sept. 2014. Available at: http://www.co2mustang.eu

Niemi, A., J. Bensabat, J. Carrera, L. Martinez Landa, L. Luquot, P. Pezard, P.Gouze, C. Juhlin, C. Cosma, M.Sauter, A.Tatomir, J.Ghergut, M.Erlström. 2014b. Recommendations for MMV-oriented implementation of field quantification and monitoring techniques MUSTANG (A multiple space and time scale approach for the quantification of deep saline formations for CO2 storage) EU FP7 project report. Deliverable 3.8. August 2014. Available at: http://www.co2mustang.eu.

Niemi, A., et al (seventy-seven co-authors). 2013. 48 Month Progress Report to the EU. MUSTANG (A multiple space and time scale approach for the quantification of deep saline formations for CO_2 storage) EU FP7 project report, Deliverable D1.1. July 2013. Available at: http://www.co2mustang.eu

Olofsson, C. 2011. The significance of heterogeneity for spreading of geologically stored carbon dioxide MSc Thesis Uppsala University, Dept. Earth Sciences. ISSN 1401-5765 June 2011.

Pearce, J. M. 2006. What can we learn from natural analogues? - An overview of how analogues can benefit the geological storage of CO_2, NATO Science Series IV Earth and Environmental Sciences, 65, 129-139.

Pezard P.A. and Anderson R.N. 1990. In situ Measurements of electrical resistivity, formation anisotropy, and tectonic context. PWLA 31st Annual Logging Symposium Lafayette (Louisiana), Paper M.

Rasmusson, K, Rasmusson, M., Fagerlund, F., Bensabat, J., Tsang, Y. and Niemi, A., 2014. Analysis of alternative push-pull-test-designs for determining in-situ residual trapping of carbon dioxide. *Int J Greenhouse Gas Control*, 27, 155-168.

Schlumberger. 2009. Schlumberger Log Interpretation Charts.

Soler,J., Luquot, L. Martinez-Perez, L. Saaltink, M., De Gaspari, F. and Carrera, J. 2016, this issue. Modeling localization in reactive transport: a case study of the Heletz laboratory experiments. Paper under review for the MUSTANG/Heletz Special Edition of International Journal of Greenhouse Gas Control. In review.

Tatomir., A, M. Halisch, F. Duschl, A. Peche, B. Wiegand, M. Schaffer, T. Licha, J. Bensabat, A. Niemi, M. Sauter. 2016, this issue. An integrated core-based analysis for characterization of flow, transport and mineralogical parameters of the Heletz Pilot CO_2 Storage Site Reservoir. Paper under review for the MUSTANG/Heletz Special Edition of International Journal of Greenhouse Gas Control. In review.

Tsang, C-F. and C. Doughty. 2003. Multi-rate flowing fluid electric conductivity method Water Resour. Res., 39 (12) (2003), pp. 1354–1362

List of Tables

Table 1a. Depth of the reservoir layers in the injection well H18A

Layer	Lithology	Top Depth	Bottom Depth
Caprock	Shale	1572	1616
LC11	Limestone	1616	1621
Heletz Sandstones	Sandstone-K	1622	1624
	Sandstone-W	1627	1629
	Sandstone-A	1632	1641

Table 1b. Depth of the reservoir layers in the monitoring well H18B

Layer	Lithology	Top Depth	Bottom Depth
Caprock	Shale	1567.0	1610.0
LC11	Limestone	1610.0	1615.0
Heletz Sandstones	Sandstone-K	1616.5	1617.5
	Sandstone-W	1621.0	1626.0
	Sandstone-A	1627.0	1635.0

Table 2. In-situ pressure and temperature in the target reservoir

Well	Date of measurement	Depth (m)	Pressure (bar)	Temperature (C)
H37	23/03/2008	1485	136	60.55
H25	27/03/2008	1520	132	65.34

Table 3a. Heletz H-18 caprock XRD mineralogy (units in weight %) (see also Edlmann et al, 2016, this issue)

	Heletz caprock A	Heletz caprock B	Heletz caprock C	Heletz caprock D	Heletz caprock E	Heletz caprock F
Quartz	1.6	1.9	5.1	3.6	3.2	0.3
Calcite	19.1	3.6	4.9	0.6	0.0	0.0
Dolomite	0.3	2.0	1.9	1.6	0.0	0.0
Pyrite	2.2	2.3	3.0	3.2	1.4	2.2
Plagioclase Feldspar	11.2	12.2	12.6	17.8	17.4	16.1
Gypsum	1.4	0.0	2.6	0.6	0.7	0.3
Illite Gp. Mins	5.1	11.6	10.0	2.5	4.4	6.7
Kaolinite	8.7	14.3	12.2	7.3	11.6	12.1
Chlorite IIb	3.2	5.3	6.1	2.3	6.7	4.9
Siderite	0.4	0.4	0.1	0.2	0.3	0.6
K-feldspar	35.7	33.8	29.0	54.8	48.2	46.1
Muscovite	8.9	10.9	10.0	2.1	4.9	9.9
Ankerite	2.3	1.7	2.4	3.3	1.1	0.8
	100.0	100.0	100.0	100.0	100.0	100.0

Table 3b. Heletz H-18 sandstone XRD mineralogy results (units in weight %) (see also Edlmann et al, 2016, this issue)

	Heletz sandstone (sample 1)	Heletz sandstone (sample 2)
Quartz	73.4	66.0
Calcite	0.0	0.1
Dolomite	1.8	0.3
Pyrite	1.8	2.3
Plagioclase Feldspar	3.4	4.4
Gypsum	0.4	0.4
Illite Gp. Mins	2.0	3.3
Kaolinite	1.3	5.0
Chlorite IIb	0.7	2.0
Siderite	1.0	0.5
K-feldspar	11.1	12.9
Muscovite	1.1	1.3
Ankerite	2.1	1.5
	100.0	100.0

Table 4. Petrophysical characteristics of a sandstone sample tested by University of Edinburgh (see also Edlmann et al, 2016, this issue)

Sample	Porosity (%)	Grain density (g/cc)	Bulk density (g/cc)	Klinkenberg permea bility (mD)
Caprock				
H-18 sample A	7.78	2.62	2.41	4.4
H-18 sample B	10.82	2.67	2.38	
H-18 sample C	8.36	2.69	2.46	
H-18 sample E	8.81	2.48	2.28	
H-18 sample F	5.75	2.87	2.07	21.9 (hairline fracture)
Reservoir rock				
Reservoir rock, layer A, depth 1634 m, medium to coarse grained	27.94	2.87	2.07	

Table 5. Water quality data from well Heletz H-18A.

Analysis	Units	Value
Ph	-	6.5
Alkalinity	$mg/L\ as\ C_aCO_3$	219
Bicarbonate	$mg/L\ as\ C_aCO_3$	219
Carbonate	$mg/L\ as\ C_aCO_3$	< 1
Dissolved oxygen	mg/L	NA
EC	$\mu S/cm$	80,500
Mineral Oil	mg/L	NA
Chloride	mg/L	30,765
Sulfate	mg/L	819
TSS – total suspended solids	mg/L	56493
TRPH by IR	mg/L	NA
Metals via ICP		
Ag	mg/L	< 0.05
Al	mg/L	5
As	mg/L	< 0.1
B	mg/L	33
Ba	mg/L	3
Be	mg/L	< 0.05
Ca	mg/L	2022
Cd	mg/L	< 0.05
Co	mg/L	< 0.05
Cr	mg/L	0.1
Cu	mg/L	5
Fe	mg/L	99
Hg	mg/L	< 0.05
K	mg/L	751
Li	mg/L	2
Mg	mg/L	548
Mn	mg/L	1
Mo	mg/L	< 0.05
Na	mg/L	19,707
Ni	mg/L	< 0.05
P	mg/L	1
Pb	mg/L	2
S	mg/L	298
Se	mg/L	< 0.05
Sn	mg/L	< 0.1
Sr	mg/L	44
Ti	mg/L	0.2
V	mg/L	< 0.05
Zn	mg/L	4
PAH by GC-MS – Not found within the detection limits		
VOC – by GC-MS-HS – not detected except for the following components		
Benzene	$\mu g/L$	11
Carbon Tetrachloride	$\mu g/L$	16

The chemical analyses were conducted at the Aminolab chemical laboratories (Ness Tsiona, Israel).

Table 6: Summary of the porosity measurements and estimates of Heletz sandstones by various groups and methods

Group doing the Experiment	**Range of values (%)**	**Represented Area**	**Represented layer**	**Data**	**# of tests**	**Reference**
GII	15-20 18 20 17	Area of the experiment Entire Heletz Formation	A,W A W K	Old data from oil exploration, geophysical well logs and cores	~40 wells	
Uni Göttingen	19-22	Area of the experiment	A	New cores, in-situ P/T conditions	5x2	Tatomir et al, 2016
CNRS	18±4 %	-’’-	A, W, K	Geophysical well logs, new wells	2	
Uni Stanford	22-25	-’’-	A	New cores, in-situ P/T conditions	~7	Hingerl et al, 2016
Uni Edinburgh	28	-’’-	A	New cores, in-situ P/T	1	Edlmann et al, 2015

Table 7. Permeability (in mD) based on measurements on two different Heletz sand cores (H18 A and B) and in two directions, atmospheric pressure conditions by LIAG /University of Göttingen group (see Niemi et al, 2014a for details)

#	Fine core (H18A), Direction I	Fine core (H18A), Direction II	Coarse core (H18B), Direction I	Coarse core (H18B), Direction II
1	449	469	339	351
2	441	465	358	343
3	431	467	355	343
4	459	453	349	342
5	449	449	343	341
6	440	456	341	339
7	426	442	348	338
8	441	453	346	335
9	455	442	348	331
10	439	447	344	329
AVERAGE	**443**	**454.3**	**347.1**	**339.2**

Table 8: Summary of the permeability measurements and estimates of Heletz sandstones by various groups and methods

Group doing the Experiment	Range of values (mD)	Well	Method	# of tests	Reference
Uni Göttingen 1[*]	440-450 340-350	H-18A H-18B	cores, atmospheric conditions	2 x 10 2 x 10	Niemi et al, 2014a
Uni Göttingen 2	325-410 180-295	H-18A H-18B	cores, in-situ P/T conditions	1 x 9 1 x 9	Tatomir et al, 2016
CNRS	100-400	H-18A	cores, in-situ P/T conditions	4	Luquot et al, 2016
Uni Stanford	104		cores, in-situ P/T conditions	1	Hingerl et al, 2016
EWRE	735 (horiz) 135 (vert)	H18-A	in-situ pumping test in the field	1	Niemi et al, 2014a,Bensabat et al, 2014

(* Including testing of anisotropy at core level

Table 9. Brooks and Corey parameters fitted to the Heletz sandstone relative permeability curves (see also Hingerl et al, 2016, this issue)

Brooks-Corey [1] fitting parameters	
Irreducible Water Saturation	0.22
Pore size distribution index λ	0.46
$k_{rco2}(s_{wi})$	0.93

Table 10: Statistical data for Heletz sand layer permeabilities

Data from entire Heletz formation			
Parameter	*Values*	*Layer*	*Data base*
μ, σ (m^2 and mD) [1] of model to log-converted data [2]	-13.25, 1.1 (log m^2) 2.1, 1.1 (log mD)	A	borehole porosity logs
-‘’-	-12.9, 1.1 (log(m^2): 1.7, 1.1 (log mD)	W	-‘’-
Data from old wells in the vicinity of experimental area			
m, s (mD) from log-converted data [3]	1.43, 0.725	Layers A,W, K	Borehole porosity logs, wells H-13, H-18 and H-38 only
Parameters for exponential model fitted to variogram data [4] a, nugget (C_0), sill (ω)	All layers 0.9,0, 0.526	-‘’-	-‘’-
Data from the new drilled wells			
Range of values (mD) [5] Range of values (log transformed, m^2)	100-410 ~-13-12.4	Layer A	Core samples, only tests with in-situ P/T conditions included
Horizontal/ Vertical permeability (mD)	735/135	Layers A, W	In-situ well test, provides an ‘upscaled’ value for the entire layer

1) Since statistical distributions of permeability are normally given in units of m2 while the rest of the analyses in this work are given in units of mD, statistics are here given in both units
2) Model parameters for the Gaussian model fitted to data
3) Mean and standard deviation determined form the data
4) Exponential model a variogram γ, as a function of lag distance h

$$\gamma(h) = C_0 + \omega\left(1 - \exp\left(-\frac{h}{a}\right)\right)$$

5) Statistics not meaningful to calculate due to the relatively small amount of data and differences in test methods, only core values measured at in-situ pressures and temperatures are included

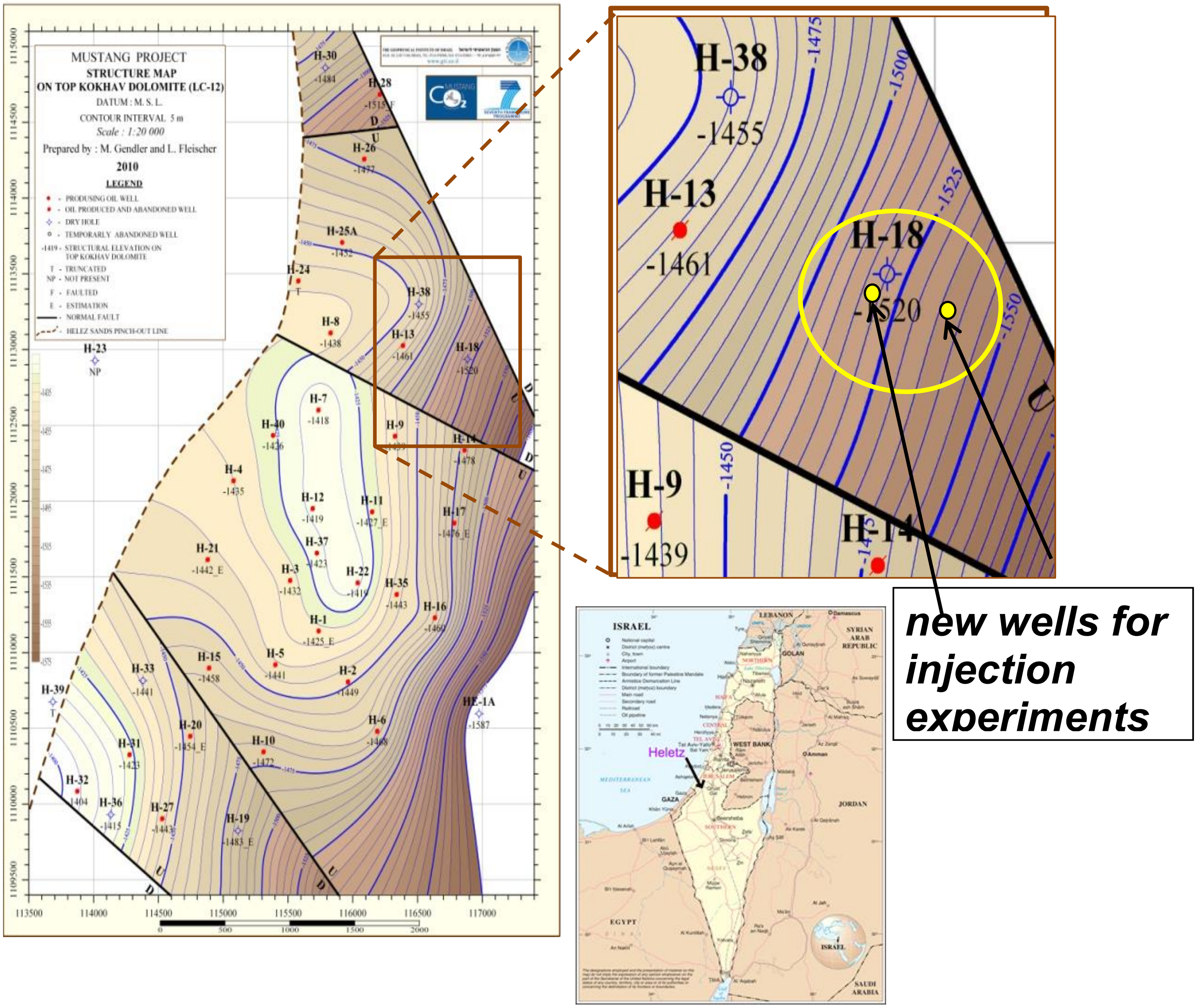

Figure 1. a) Elevation map of the bottom of the sand reservoir at Heletz, as well as the positions of the oil exploration wells along with a zoom-in to the experimental area for CO_2 injection experiments, including the location of the new drilled wells H-18A and H-18B. The map (source modified after free Wikipedia) shows the site location.

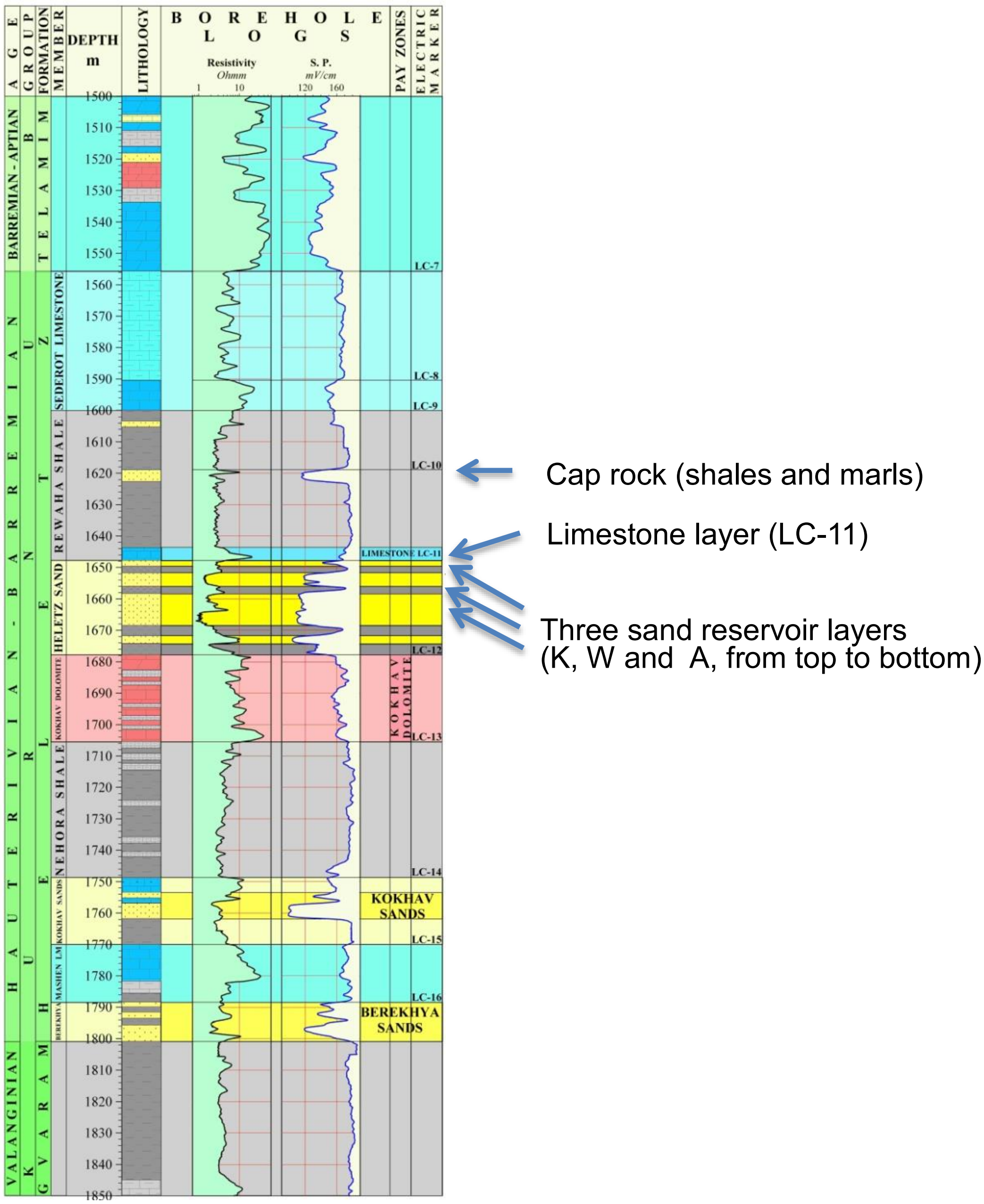

Figure 2. Type lithology at Heletz indicating the cap-rock and reservoir units (reservoir units indicated with yellow)

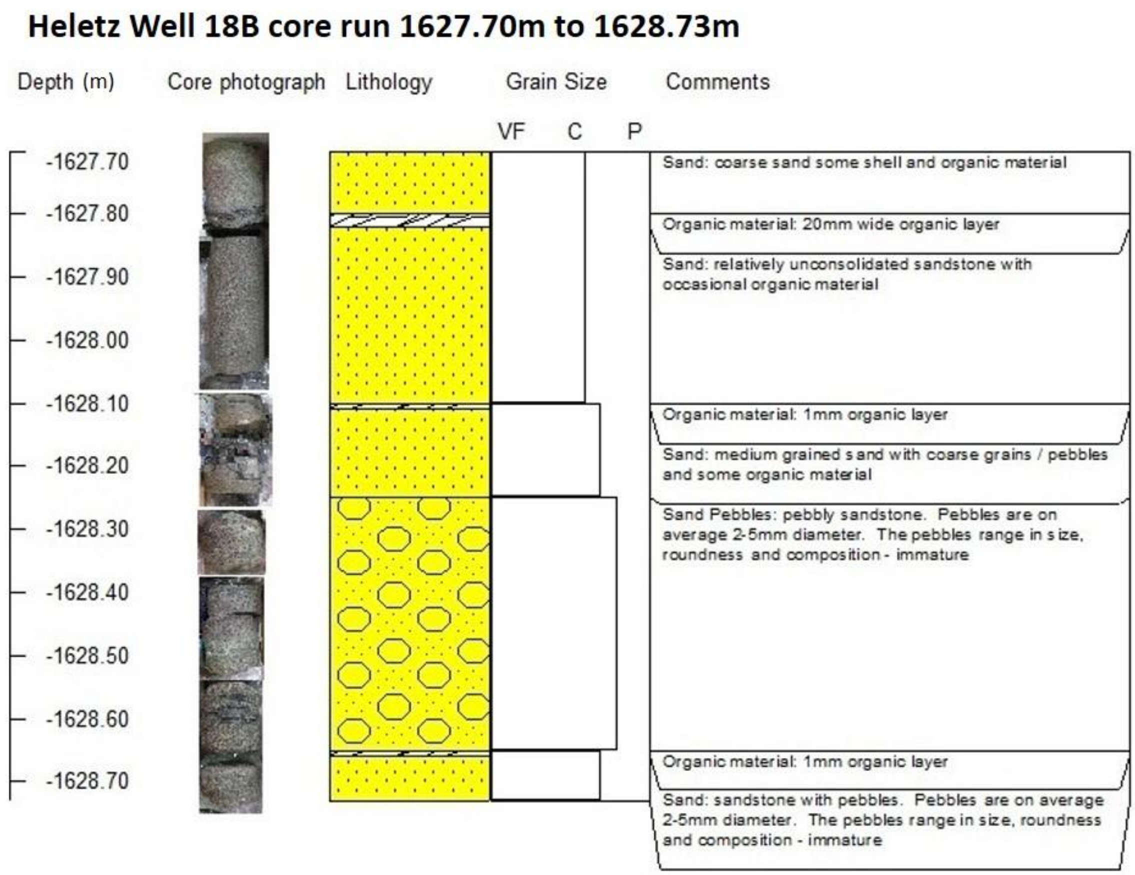

Figure 3. a) Example core run along with the interpreted lithology, H-18B, reservoir rock layer A. b) Example cores of the cap-rock in epoxy resin.

The i

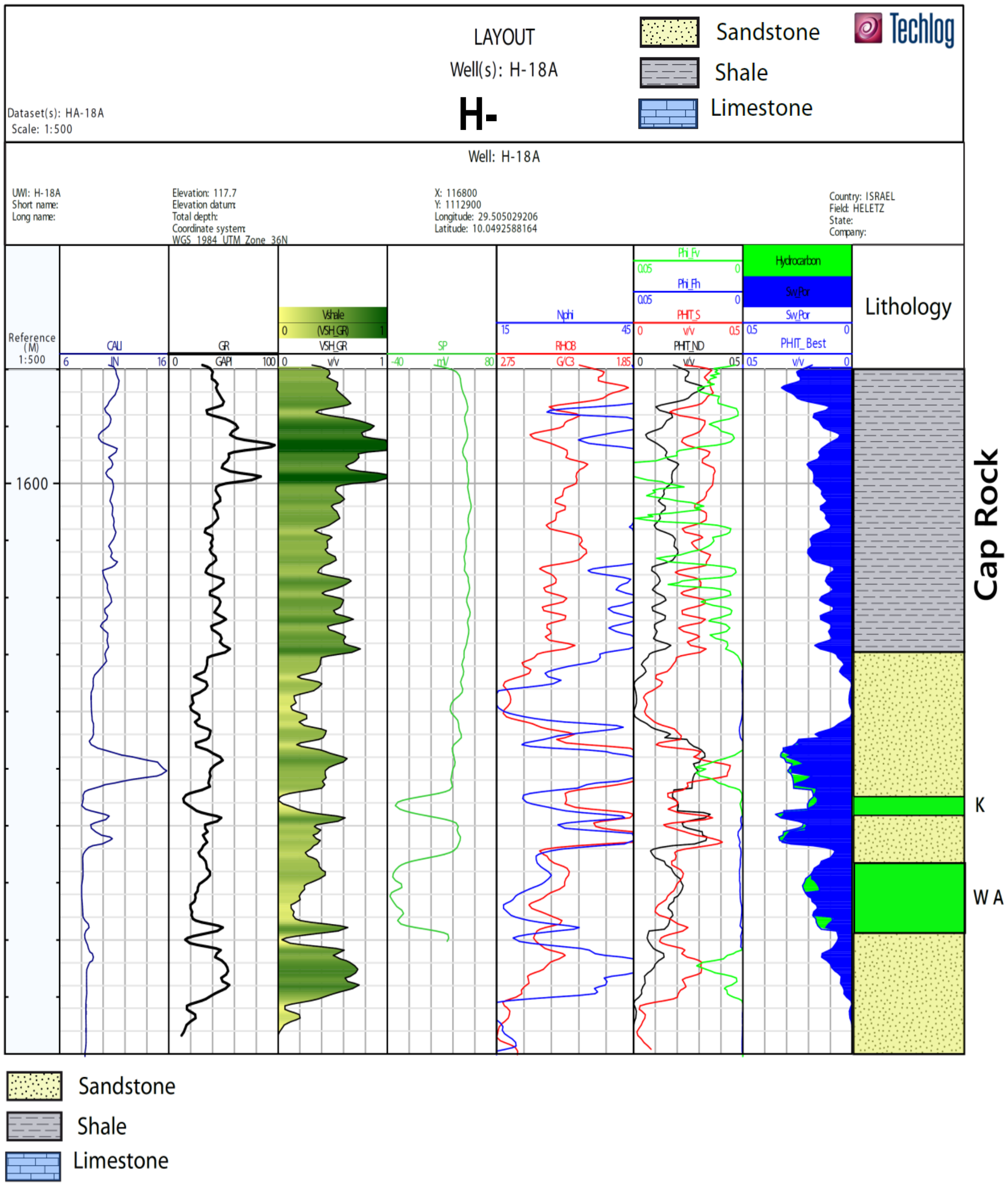

Figure 4. Examples of geophysical logs from Heletz H-18A analyzed with Techlog. From left to right: caliper (CALI, in blue), natural gamma radioactivity (GR, in black), shale content (VSh, shaded with variable green colors related to shale amount), spontaneous potential (SP, in light green), neutron porosity (NPHI in blue) and density (RHOB in red), porosity computed from acoustic Vp logging (PHIT_S in red) with H-porosity computed from neutron-density (PHIT_ND in black) and fracture porosity from dual laterolog resistivity analysis, either in light green for vertical fractures or blue for horizontal fractures. Please note that the scale is amplified by a factor of 10 for these last two fracture porosity curves with respect to previous porosity estimates. Reservoirs are indicated with green color in the right-hand side lithological column

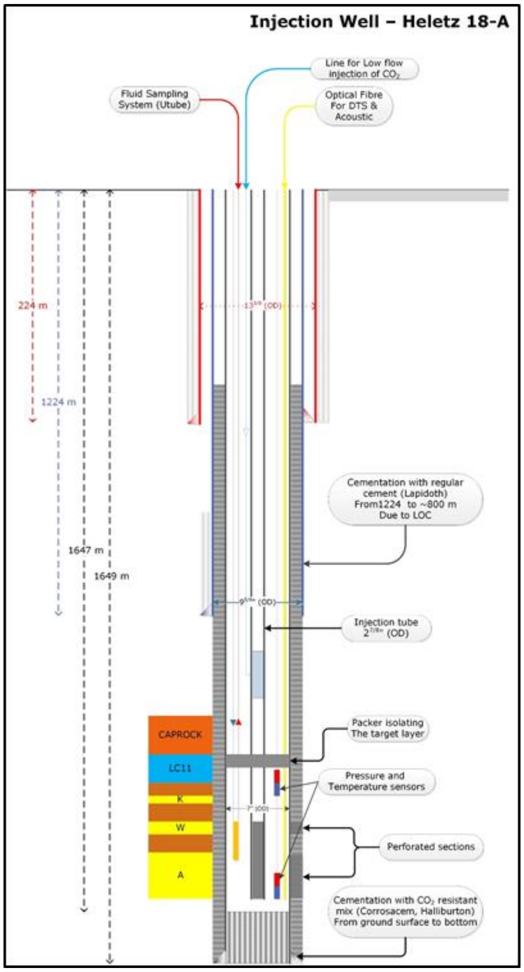
Injection Well – Heletz 18-A
Line for Low flow injection of CO2
Fluid Sampling System (Utube)
Optical Fibre For DTS & Acoustic
224 m
1224 m
1647 m
1649 m
Cementation with regular cement (Lapidoth) From1224 to ~800 m Due to LOC
Injection tube 2 7/8" (OD)
CAPROCK
LC11
K
W
A
Packer isolating The target layer
Pressure and Temperature sensors
Perforated sections
Cementation with CO2 resistant mix (Corrosacem, Halliburton) From ground surface to bottom

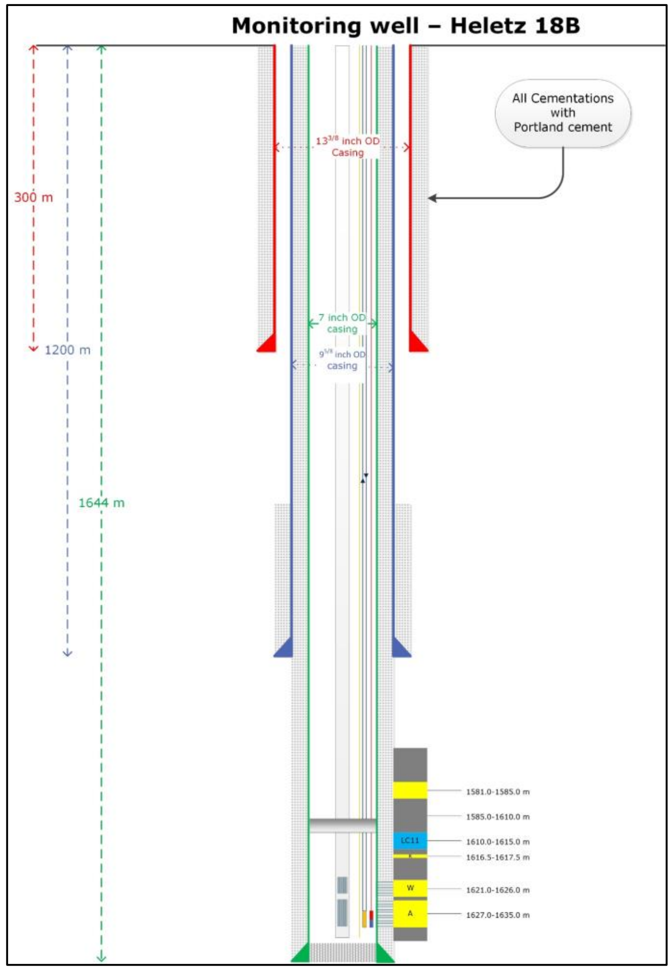
Monitoring well – Heletz 18B
All Cementations with Portland cement
13 3/8 inch OD Casing
300 m
7 inch OD casing
9 5/8 inch OD casing
1200 m
1644 m
1581.0-1585.0 m
1585.0-1610.0 m
LC11
1610.0-1615.0 m
1616.5-1617.5 m
W
1621.0-1626.0 m
A
1627.0-1635.0 m

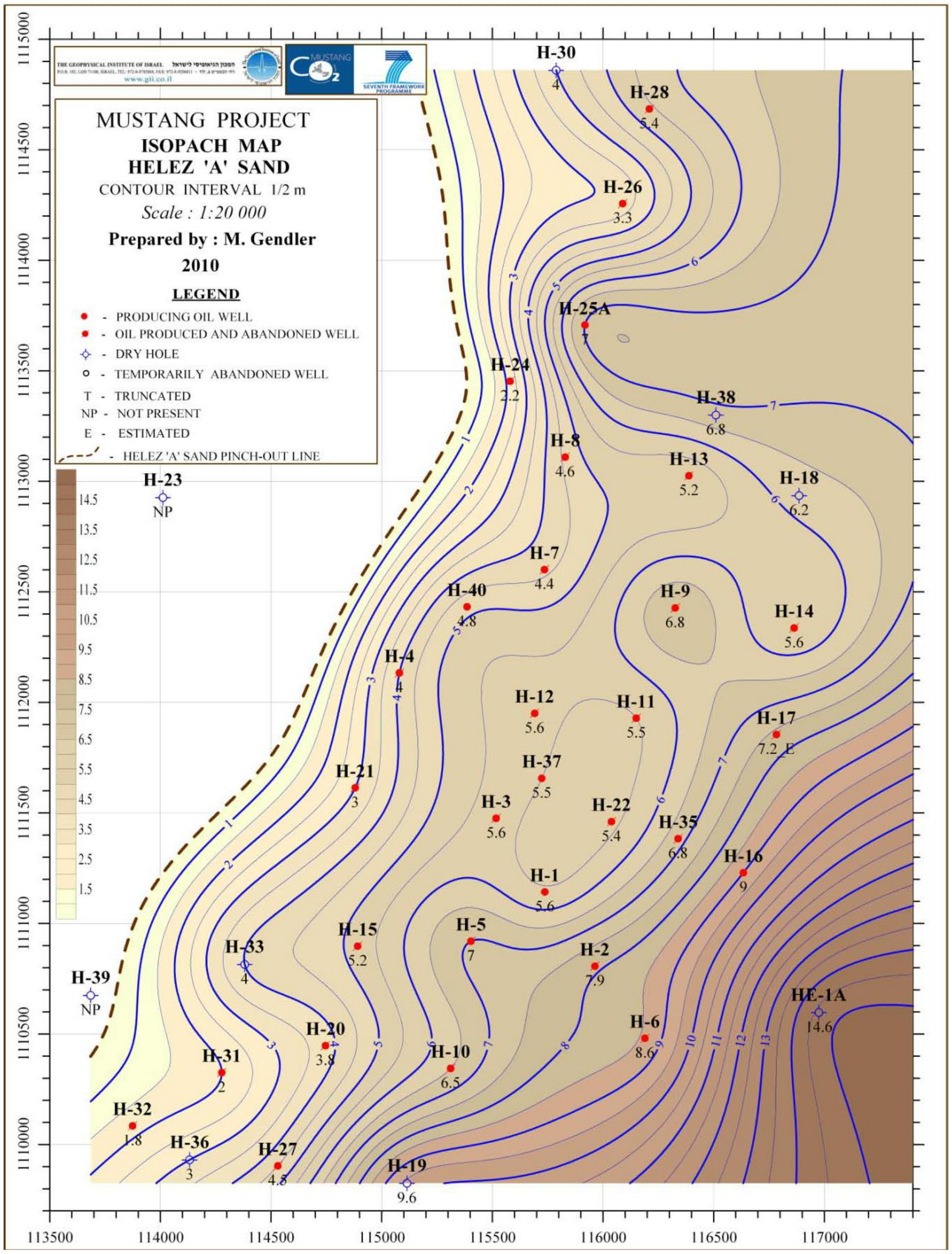

Figure 6. Example isopach map of the sand layer A at Heletz.

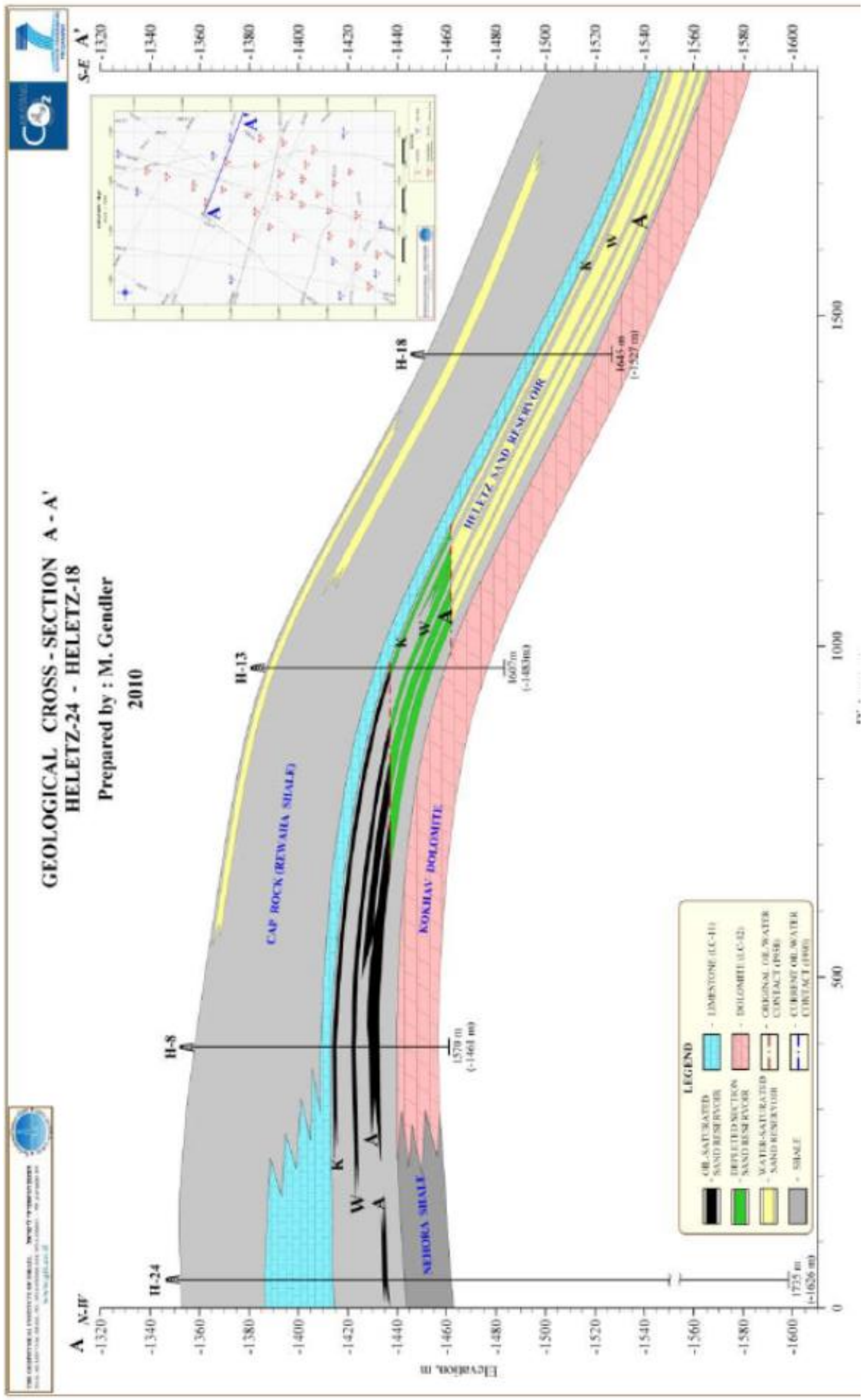

Figure 7. Example geological cross-section A-A crossing the CO_2 investigation area and well H18. Sand layers are indicated with yellow color.

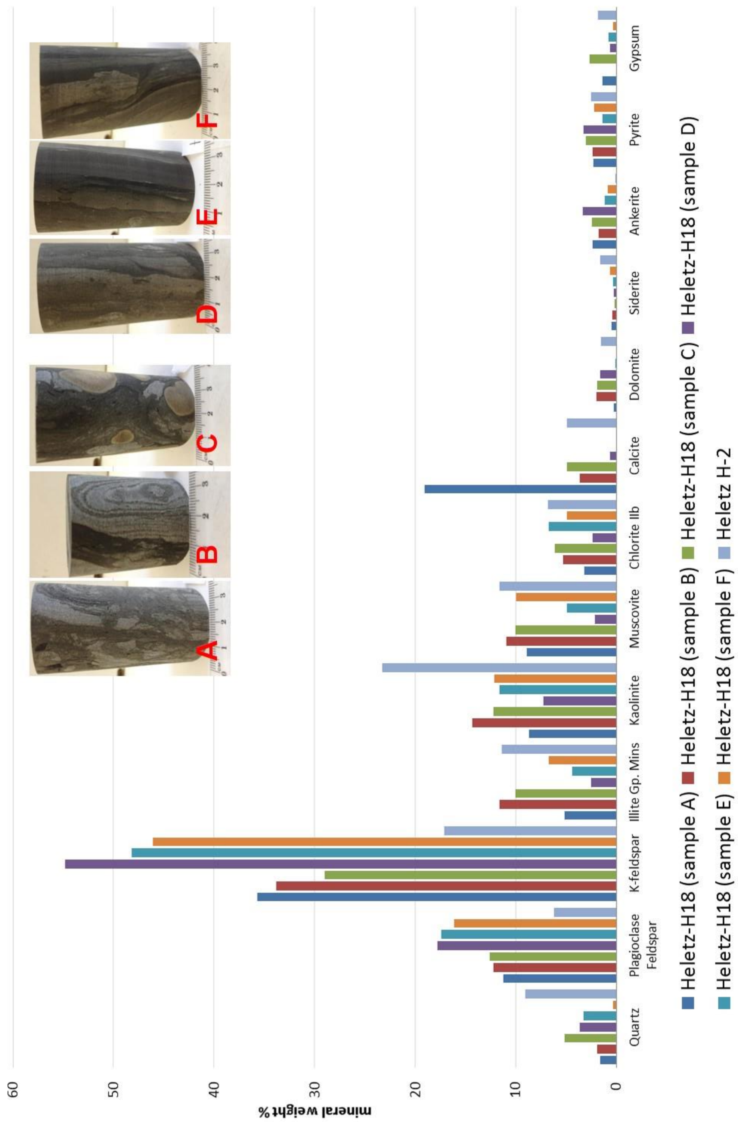

Figure 8a. Minerology of caprock samples (for more details see Edlmann et al, 2016, this issue)

Figure 8b. Minearology of sandstone samples (for more details see Edlmann et al, 2016, this issue)

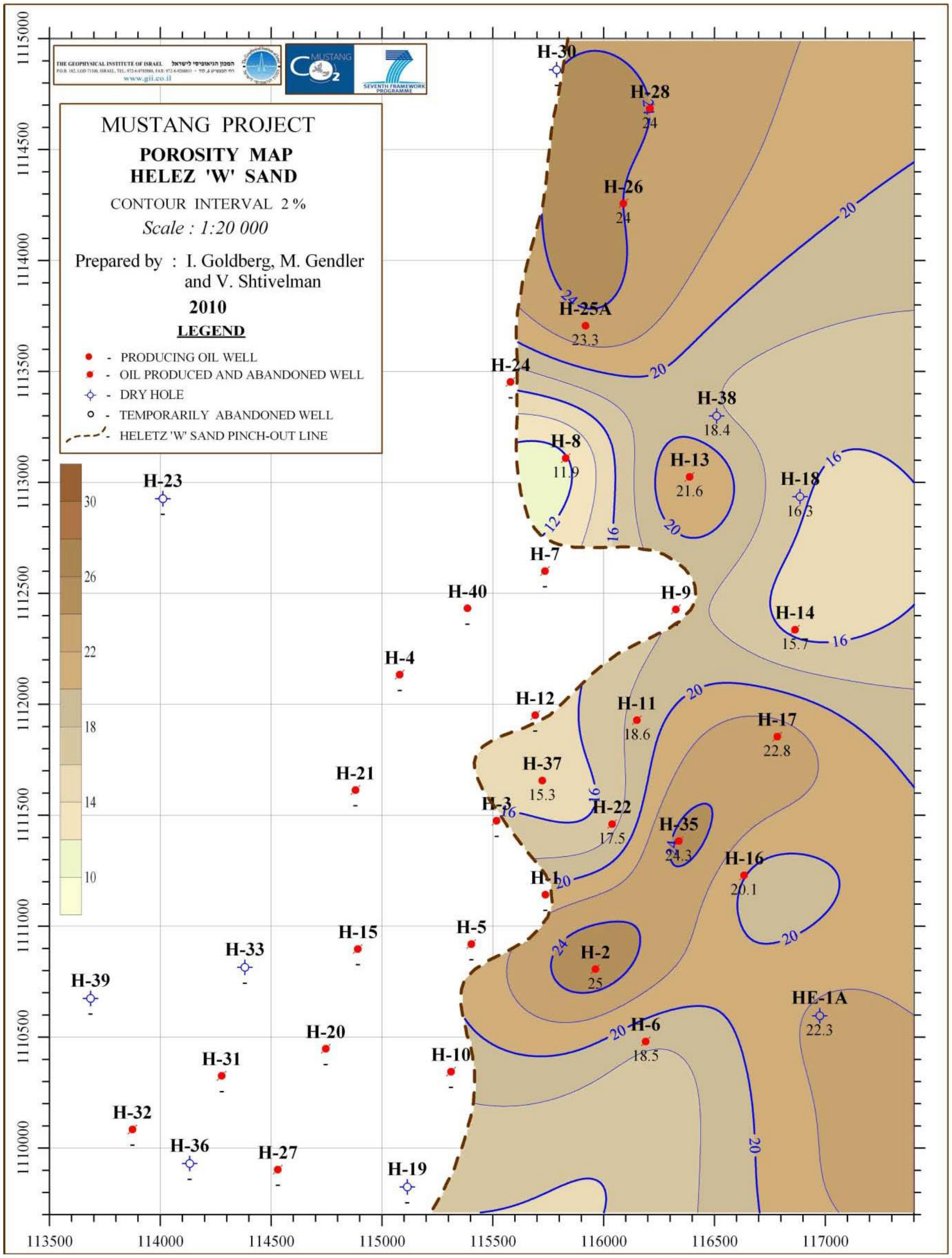

Figure 9. Porosity of reservoir layer W, estimated from well and core data from oil exploration investigations.

a)

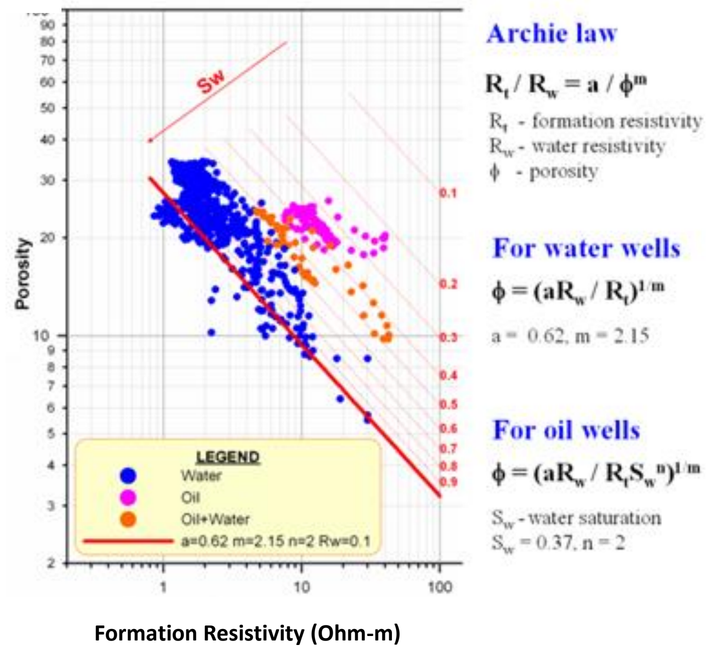

b)

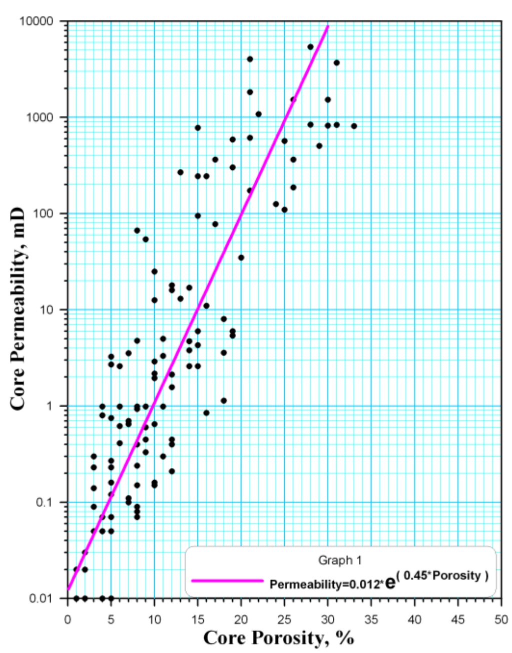

Figure 10. a) Relationship used to estimate the formation porosity from the old well data and b) porosity-permeability relationship used to determine permeability values.

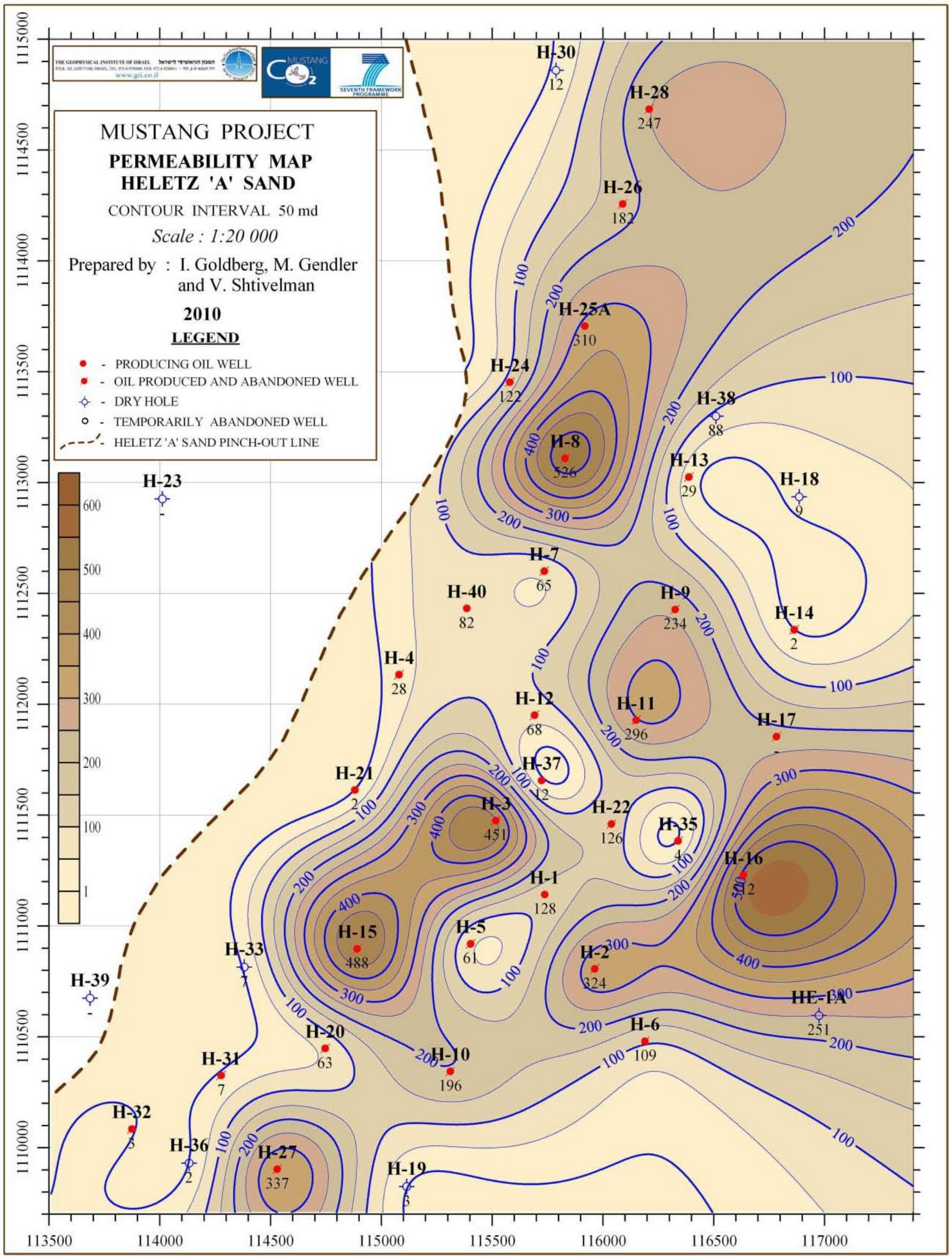

Figure 11a. Permeability of reservoir layer A, estimated from well and core data from oil exploration investigations and the porosity-permeability relationship (Fig 10).

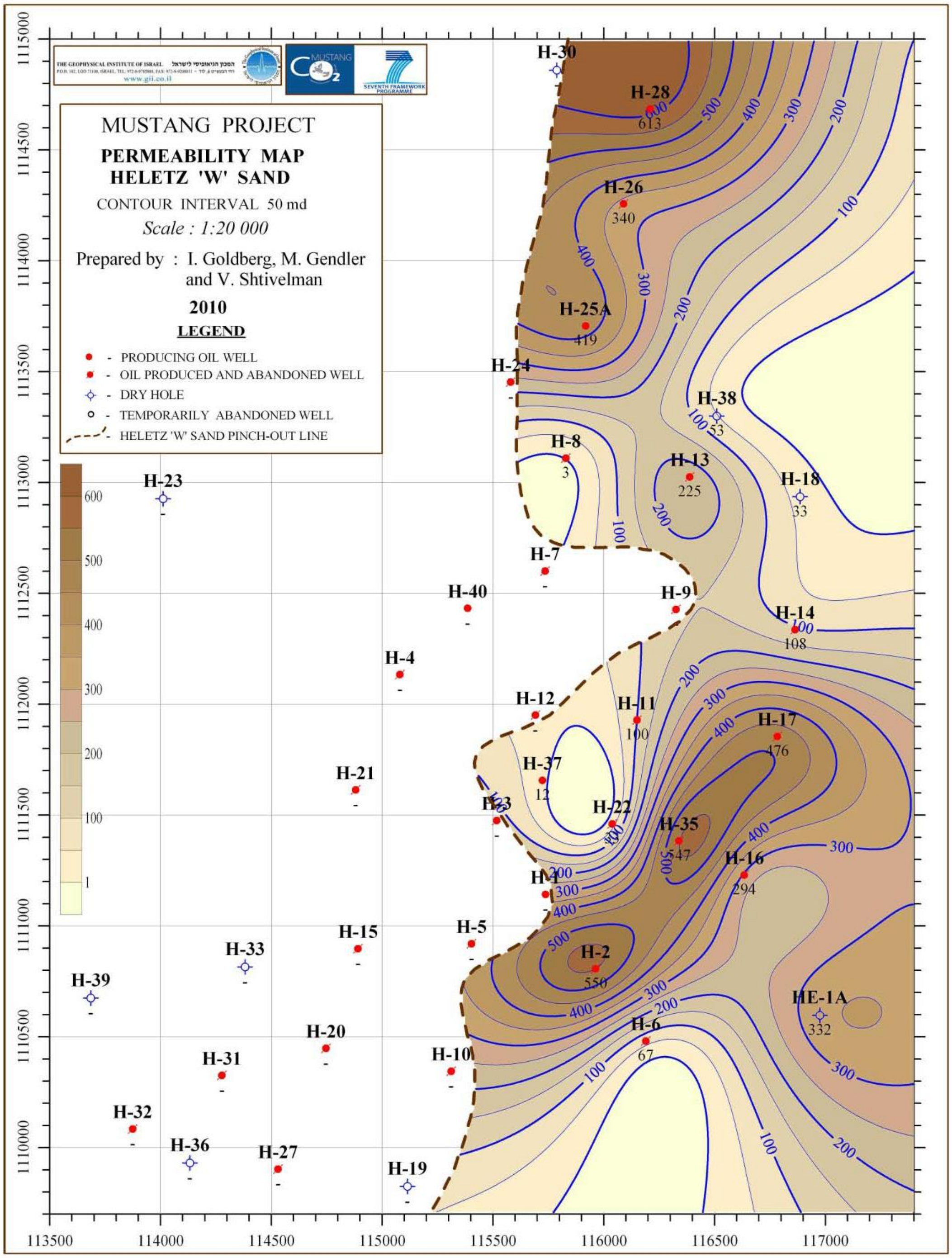

Figure 11b. Permeability of reservoir layer W, estimated from well and core data from oil exploration investigations and the porosity-permeability relationship (Fig 10).

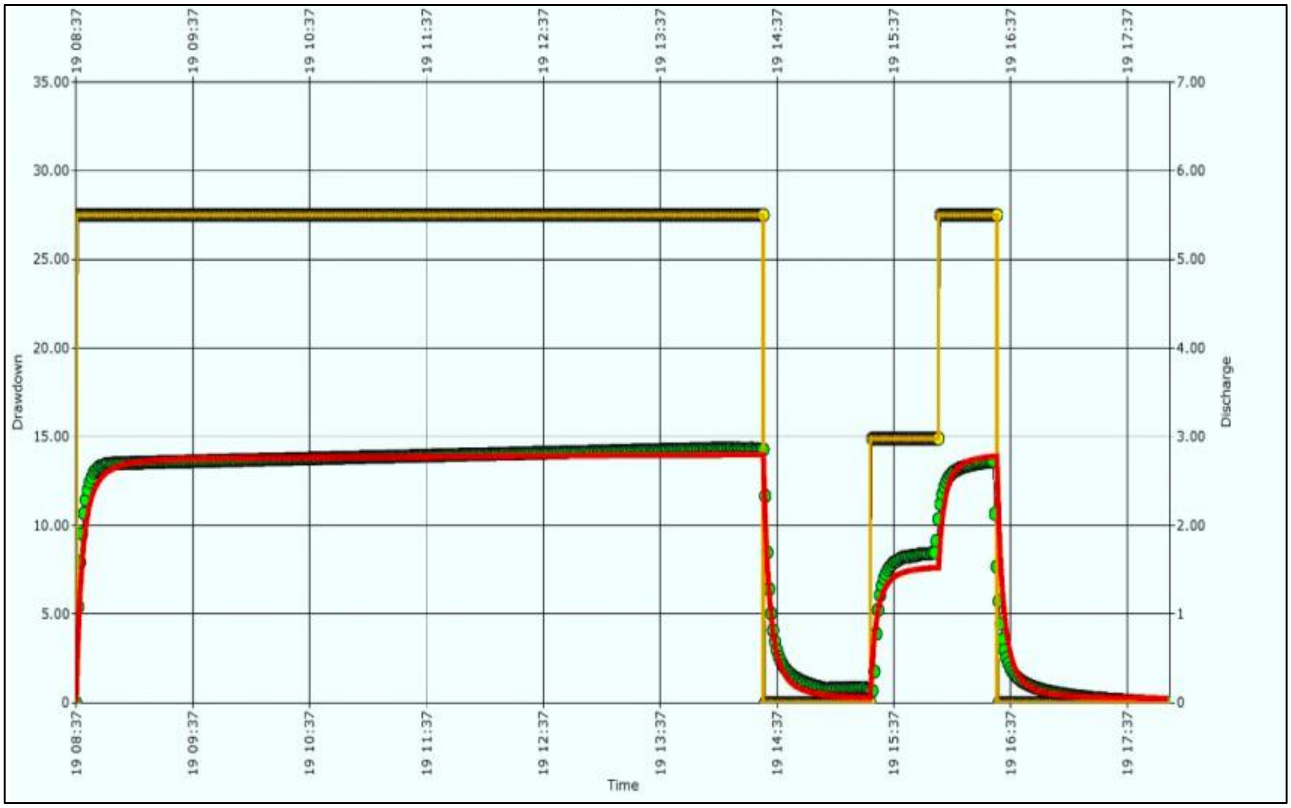

Figure 12. Drawdown (green symbols) and pumping discharge (yellow symbols) during the pumping test in well H-18A to determine in-situ permeability for reservoir layers.

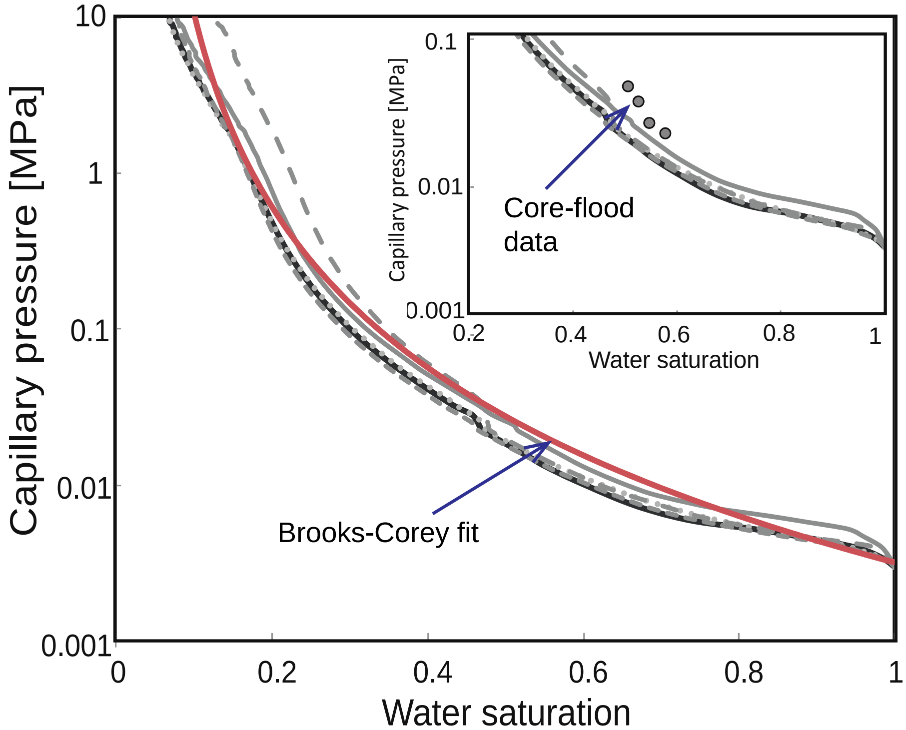

Figure 13. Capillary pressure curve measured on 6 sub-samples using Mercury Intrusion Porosimetry. Data were converted to the system supercritical (sc) CO_2/H_2O using a wetting angle for supercritical CO_2-H_2O-rock of 0 degree and an interfacial tension between CO_2 and H_2O of 0.035 N/m. A Brooks-Corey fit to the data is shown by the red curve. Additional capillary pressure data obtained using multi-phase core flooding are indicated by filled circles. The figure inlet depicts the capillary pressure range relevant for CO_2 sequestration.

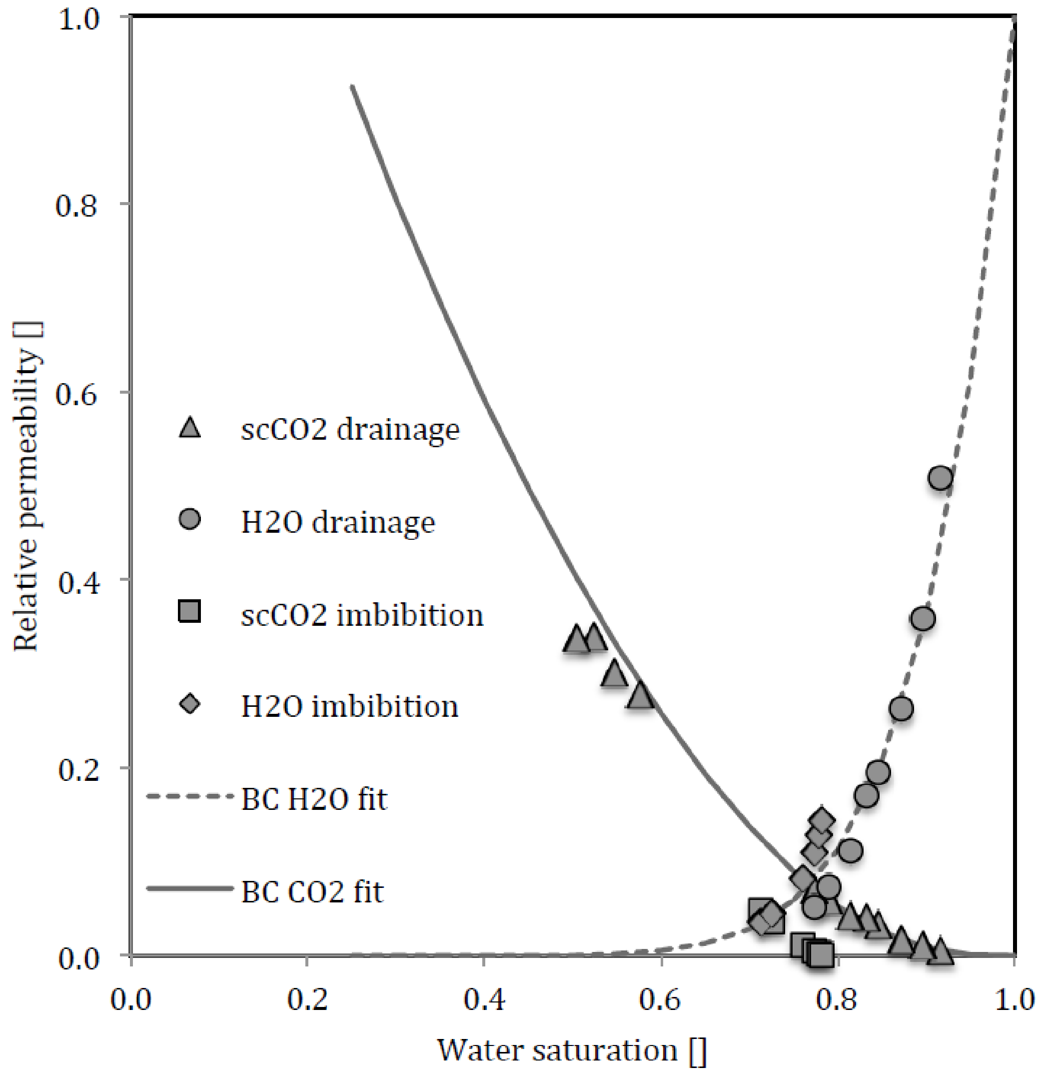

Figure14. Drainage and imbibition relative permeability curves for a sample from sandstone (A layer) a) the data and b) model fitting by Benson et al (2014).

For the details of the measurements see Hingerl et al. (2016). Working fluids are supercritical CO_2 and water at 10.3 MPa pressure and 50 C.

a)

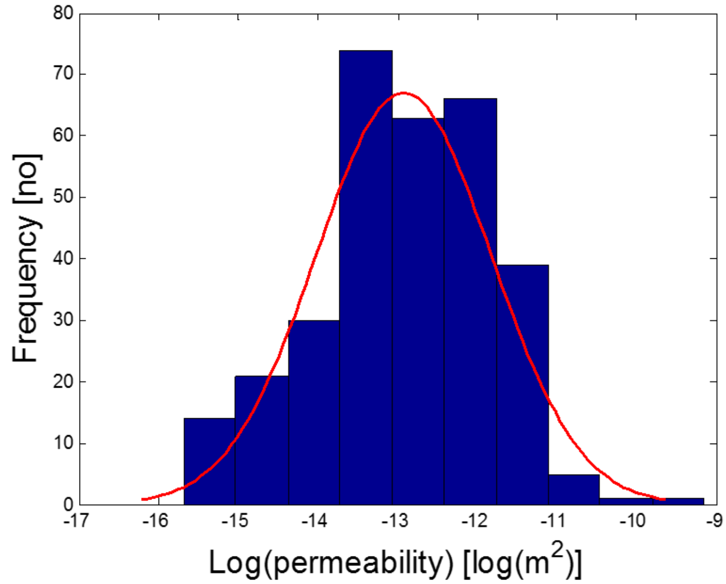

b)

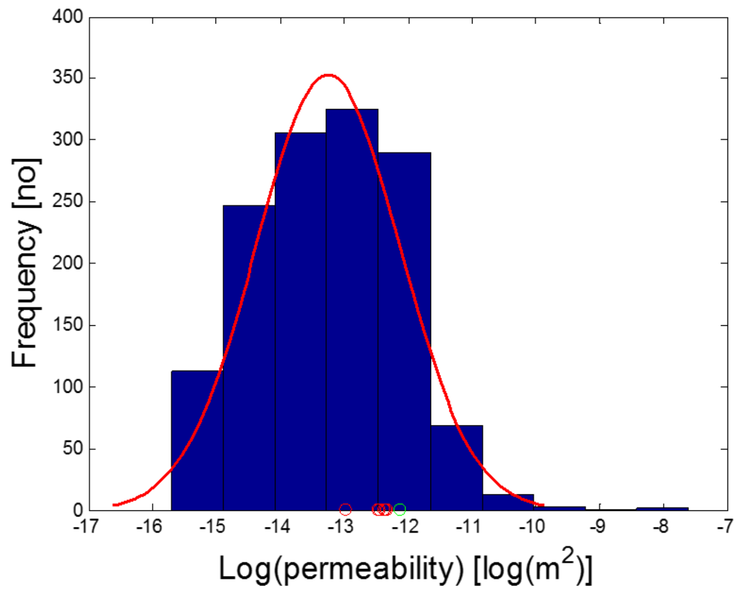

Figure 15. Histogram of permeabilities for Heletz layers W and A, based on original oil wells porosities and the porosity-permeability relationship in Figure 10. The range of values measured from wells H-18A and H-18 is indicated with the red dots and the value form the well test with the green dot.

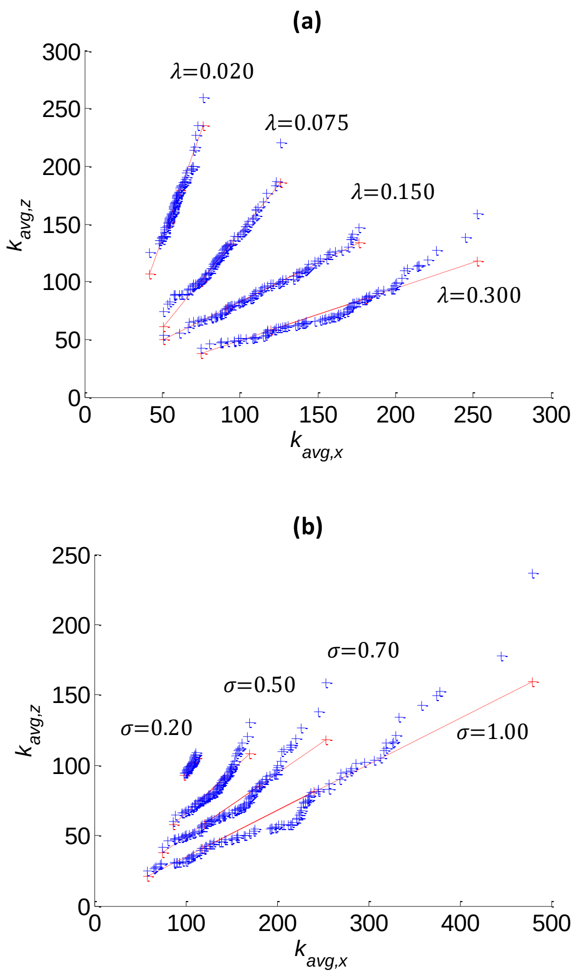

Figure 16. Domain upscaled permeabilities (Unit: mD). (a) Effects of varying λ with fixed σ = 0.70; (b) Effects of varying σ with fixed λ = 0.30 (30m); The symbols show the result from the various realizations. The model dimensions are 10 m x 100m, mean permeability 100 mD and λ is given as ratio of the total horizontal length, i.e. λ = 0.30 corresponds to 30m vertical correlation length constant 3m.

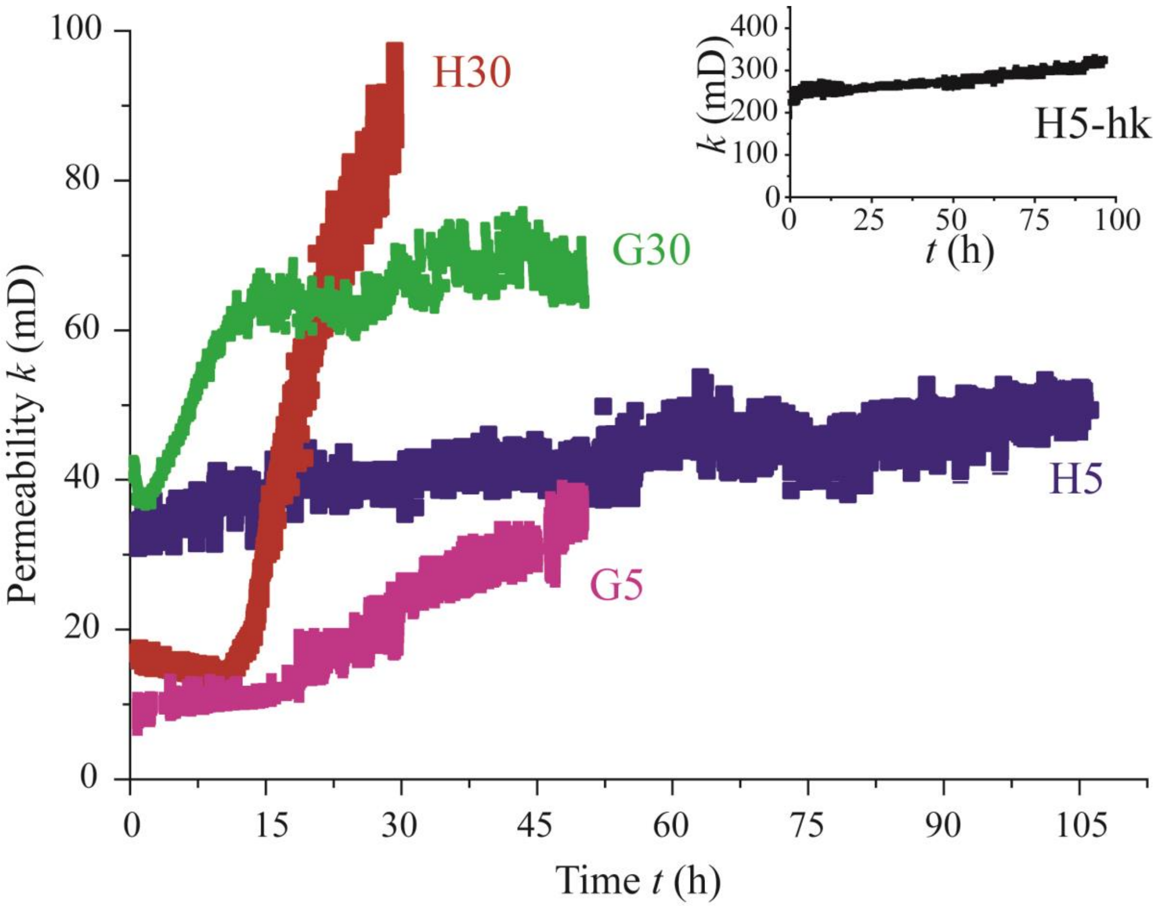

	Q (ml/min)	Brine
H5-hk	0.05	Heletz Brine (H-Type)
H5	0.05	Heletz Brine (H-Type)
H30	0.30	Heletz Brine (H-Type)
G30	0.30	Heletz Brine eq, Gypsum (G-Type)
G5	0.05	Heletz Brine eq, Gypsum (G-Type)

Figure 17. Changes in core permeabilities when in contact with brines saturated with CO_2, for different injection flow rates and brine compositions. For experiment details see Luquot et al. (2016, this issue)

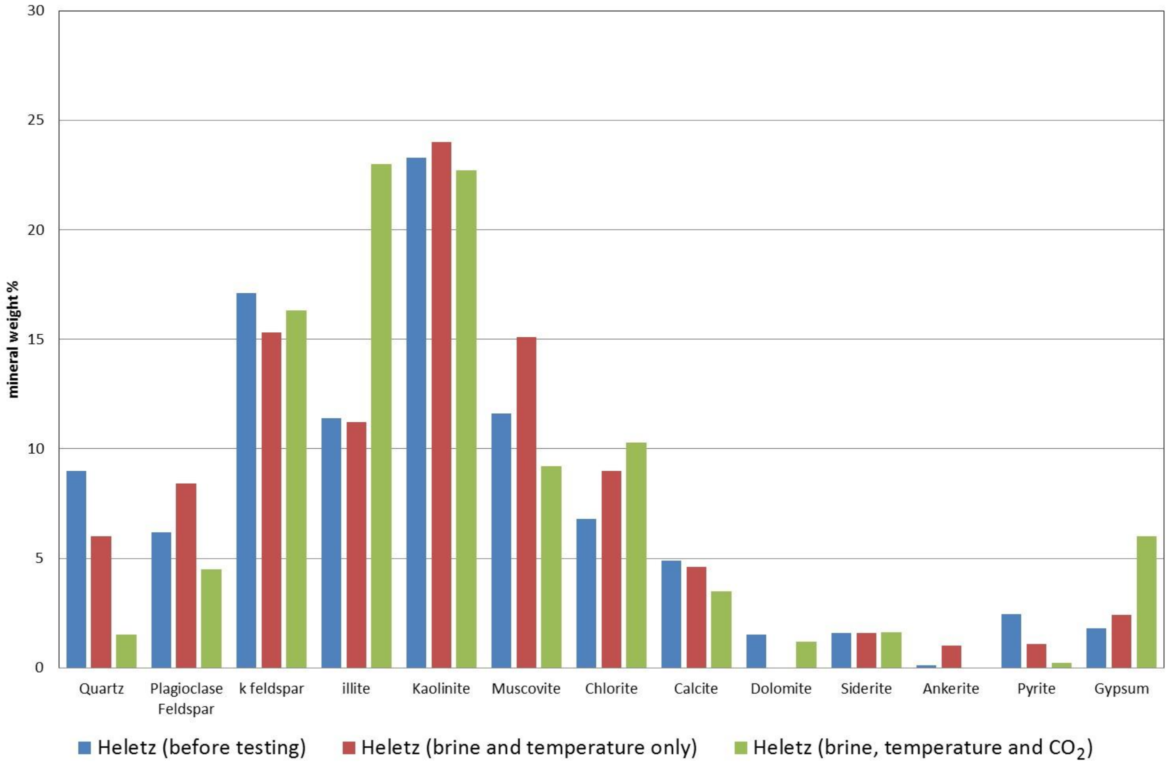

Figure 18. Changes in cap-rock mineralogy when in contact with CO_2 saturated brine, for experiment details see Edlmann et al. (2016, this issue)